



Contents lists available at ScienceDirect

## International Journal of Heat and Mass Transfer

journal homepage: [www.elsevier.com/locate/ijhmt](http://www.elsevier.com/locate/ijhmt)

# Near-interface effects on interfacial phonon transport: Competition between phonon-phonon interference and phonon-phonon scattering

Yixin Xu<sup>a</sup>, Bing-Yang Cao<sup>b,\*</sup>, Yanguang Zhou<sup>a,\*</sup>

<sup>a</sup> Department of Mechanical and Aerospace Engineering, The Hong Kong University of Science and Technology, Clear Water Bay, Kowloon, Hong Kong SAR

<sup>b</sup> Key Laboratory of Thermal Science and Power Engineering of Ministry of Education, Department of Engineering Mechanics, Tsinghua University, Beijing 100084, China

## ARTICLE INFO

## Keywords:

Interfacial phonon transport  
Phonon couplings  
Near-interface  
Phonon interference  
Phonon scatterings

## ABSTRACT

Recent studies suggest that the phonon-phonon couplings in the near-interface region may affect interfacial thermal transport. In this paper, we revisit the interfacial thermal transport considering phonon-phonon couplings across the interface and in the near-interface region. We find that phonon-phonon couplings in the near-interface region show a dual influence on the interfacial thermal transport. On the one hand, the phonon-phonon couplings in the near-interface region will benefit the interfacial thermal transport via phonon-phonon interference. On the other hand, the phonon-phonon couplings in the near-interface region hinder the interfacial thermal transport through phonon-phonon scatterings. Mechanical-contacted and chemical-bonding Cu/Si interfaces are chosen as examples to investigate interfacial thermal transport. For mechanical-contacted Cu/Si interfaces, the interfacial thermal transport is dominant by the phonon-phonon couplings across the interface. The influence of phonon-phonon couplings in the near-interface region on interfacial thermal transport could be ignored. For chemical-bonding Cu/Si interfaces, phonon-phonon couplings in the near-interface region can contribute as high as 10 % (7 % with quantum corrections) to interfacial thermal transport at low temperatures (i.e., < 300 K). This is because the interference among these phonons in the near-interface region is stronger than their corresponding scatterings. At high temperatures (i.e., > 300 K), the phonon-phonon scatterings in the near-interface region become more important and surpass the corresponding interference. Consequently, the phonon-phonon couplings in the near-interface region will hinder interfacial thermal transport. Our work here quantifies the influence of phonon-phonon couplings in the near-interface region on interfacial thermal transport, which advances the fundamental understanding of interfacial thermal conduction.

## 1. Introduction

Interfacial thermal transport is essential to the thermal management in microelectronics, which has become one of the major bottlenecks to the continued scaling of microelectronics for the next generation and beyond as microelectronics become increasingly smaller with higher power density. The prediction of interfacial thermal conductance (ITC) requires an understanding of heat carriers' properties and their scattering mechanisms at the interface. In 1959, Little [1] proposed the acoustic mismatch model (AMM) to access the interfacial thermal transport, which assumed all phonons elastically transferred across the interfaces. Swartz and Pohl [2] then proposed the diffuse mismatch model (DMM) by considering the incident phonons were completely scattered diffusively. Therefore, the DMM inherently excludes the wave nature of phonons [3], which leads to an underestimation of the

contribution of low-frequency phonons for predicted ITC [4]. Furthermore, atomistic Green's function (AGF) [5] was developed to solve the phonon transfer across the solid/solid interfaces based on the phonon gas model (PGM) [6]. All these methods mentioned above consider the interfacial thermal transport via phonon-phonon couplings across an ideal interface with no thickness. The corresponding heat flux across this ideal interface can be expressed as the phonon transmission function [7]. It is assumed that the temperature difference between the left and right contacts is infinitesimal, and the temperatures of both sides approach to  $T$  [7]. Combining with the Landauer transport theory [3], the interfacial thermal conductance can be evaluated by

\* Corresponding authors.

E-mail addresses: [caoby@mail.tsinghua.edu.cn](mailto:caoby@mail.tsinghua.edu.cn) (B.-Y. Cao), [maeygzhou@ust.hk](mailto:maeygzhou@ust.hk) (Y. Zhou).

<https://doi.org/10.1016/j.ijheatmasstransfer.2024.125943>

Received 28 March 2024; Received in revised form 1 July 2024; Accepted 6 July 2024

Available online 18 July 2024

0017-9310/© 2024 Elsevier Ltd. All rights reserved, including those for text and data mining, AI training, and similar technologies.

$$\begin{aligned}
G(T) &= \lim_{T_L, T_R \rightarrow T} \int_0^{\omega_{cut-off}} \frac{\hbar\omega [f_L(\omega, T_L) - f_R(\omega, T_R)] \cdot \Gamma(\omega, T)}{A(T_L - T_R)} d\omega \\
&= \lim_{T_L, T_R \rightarrow T} \int_0^{\omega_{cut-off}} \frac{\hbar\omega \Delta f(\omega, T) \cdot \Gamma(\omega, T)}{A \Delta T} d\omega \\
&\approx \int_0^{\omega_{cut-off}} \frac{\hbar\omega \cdot \Gamma(\omega)}{A} \frac{\partial f(\omega)}{\partial T} d\omega
\end{aligned} \quad (1)$$

where  $f(\omega, T)$  is the equilibrium phonon distribution function following the Bose-Einstein distribution, i.e.,  $f(\omega, T) = [e^{\hbar\omega/k_B T} - 1]^{-1}$ ,  $k_B$  denotes the Boltzmann constant,  $\hbar$  is the reduced Planck constant,  $\omega$  is the phonon frequency,  $\Gamma(\omega, T)$  is the phonon transmission function, and  $A$  is the cross-section area, and  $\Delta T$  is the temperature difference between two contact leads (i.e., the left and right lead).

Consequently, the estimation of interfacial thermal transport is then simplified to solve the phonon transmission coefficient, as implemented in AMM [1], DMM [2], and AGF calculations [5]. However, the phonon-phonon couplings in the near-interface region are usually ignored when using these methods, which may affect the phonon occupation and the corresponding transmission coefficient. For instance, Feng *et al.* [8] showed that the phonon distribution in the near-interface region significantly deviated from that in their bulk counterpart and provided a significant additional thermal interfacial resistance mechanism besides phonon-interface reflection. Recent studies showed that the localized phonon modes [9–11] could contribute to the ITC, mainly via their correlation with other traveling phonons that extend in the materials [12,13]. Zhou *et al.* [11] further demonstrated that these near-interface phonon couplings between localized modes and traveling modes significantly changed the transmission of traveling phonons and, therefore, affected the ITC. While there were both experimental observations [9,10] and theoretical studies [11,12,14] showing the phonon-phonon couplings in the near-interface affect interfacial thermal transport, the underlying mechanisms for the influence of near-interface phonons on interfacial thermal conduction remain unclear.

In this work, we choose two typical types of interfaces, i.e., the mechanical-contacted Cu/Si interface, which can be described by Lennard-Jones (LJ) potential [15,16], and the chemical-bonding Cu/Si interface, which is depicted by the many-body Tersoff potential [17,18], to investigate the near-interface effect on interfacial thermal transport. In this paper, we apply the phonon concept to describe the normal modes in molecular dynamics (MD), which is widely acceptable [19]. Our results show that the interfacial thermal transport at both

mechanical-contacted and chemical-bonding interfaces is affected by the phonon-phonon couplings and phonon non-equilibrium distribution in the near-interface region. The phonon-phonon couplings represent the phonon-phonon interactions that include both phonon scatterings (i.e., both elastic and inelastic) and phonon interference. On the one hand, the phonons are treated as free "gas" particles when their lifetimes are much longer than their corresponding oscillation periods, which is based on the phonon-gas theory [20]. These phonon modes carried heat from the left bulk side (e.g.,  $\lambda_{L1}(\omega)$  in Fig. 1a and  $\lambda_{L1}(\omega_1)$  in Fig. 1b) are scattered by the phonons in the near-interface region, and thus redistribute the heat among these phonons (e.g.,  $\lambda_{L2}(\omega)$  in Fig. 1a,  $\lambda_{L2}(\omega_2)$  and  $\lambda_{L3}(\omega_3)$  in Fig. 1b). The phonon-phonon scatterings in the near-interface region as stated here, represent these phenomena, which has been demonstrated by other references [9,11,21]. As a result, the heat flux across the interface is changed by the phonon-phonon scatterings in the near-interface region. For example, the heat flux carried by phonon mode  $\lambda_{L1}(\omega)$  is transferred to phonon mode  $\lambda_{R2}(\omega)$  when the near-interface effect is ignored (dashed line in Fig. 1a). However, the heat flux carried by phonon mode  $\lambda_{L1}(\omega)$  will be transferred to phonon mode  $\lambda_{L2}(\omega)$  then phonon mode  $\lambda_{R1}(\omega)$ , and eventually to phonon mode  $\lambda_{R2}(\omega)$  when the near-interface effect is considered (solid lines in Fig. 1a).

On the other hand, the wave behavior of the phonon quasiparticles is important when their lifetimes are comparable to their oscillation periods (i.e., low-frequency or equivalently long-wavelength phonons in our study). It has been demonstrated that long-wavelength phonon modes will interfere with the extended phonon modes and then benefit the propagation of these extended phonon modes [22]. When a phonon (i.e., wave) is incident on the near-interface region, multiple reflected phonons are then created in the near-interface region (Fig. 1c). If these waves are in the same phase, they interfere constructively with each other and thus form a wave packet that will facilitate the interfacial thermal transport (Fig. 1d). The phonon interference (also referred as phonon coherence [22–24]) will facilitate the thermal transport has been observed in many experiments [25,26] and simulations [22,27].

By performing the spectral heat current decomposition in the frame of non-equilibrium molecular dynamics (NEMD) simulations and phonon correlation analysis, we systematically study the phonon-phonon couplings across the interface and in the near-interface region. We further investigate the influence of temperature on the interfacial thermal transport, in which the phonon-phonon couplings in the near-interface region are found to be strongly correlated to temperature. The phonon-phonon couplings in the near-interface region can either

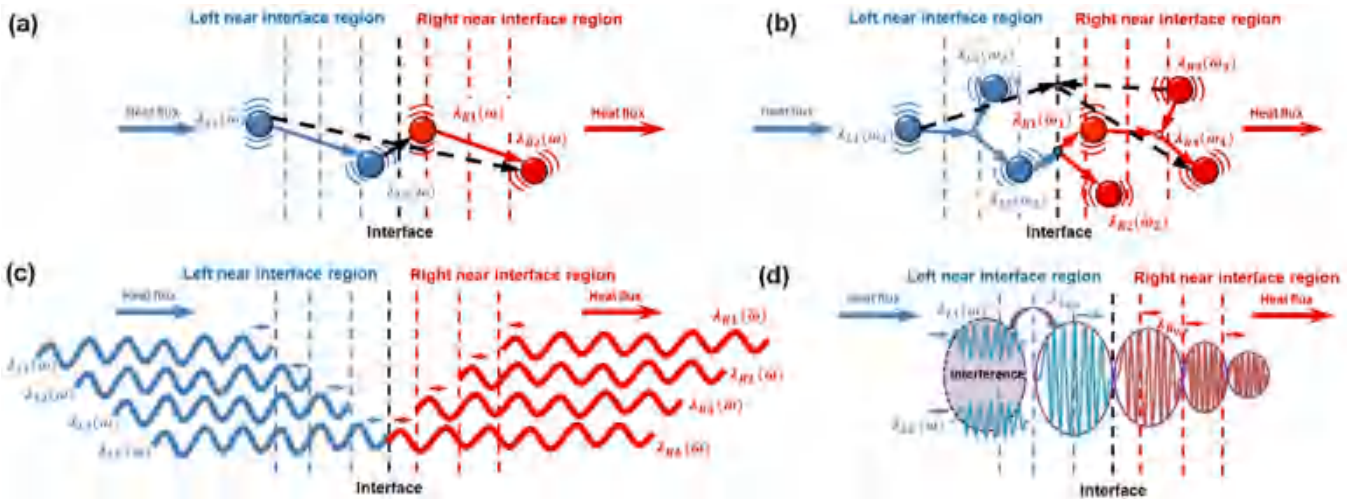


**Fig. 1.** Schematic for phonon-phonon couplings across the interface and in the near interface region. (a) The elastic phonon-phonon scatterings. (b) The inelastic phonon-phonon scatterings. (c) The incident phonon modes and reflected phonon modes in the near interface region. (d) Interference between incident phonon modes and reflected phonon modes in the near interface region.

hinder or benefit the interfacial thermal transport depending on the competition between the phonon-phonon scattering and the phonon-phonon interference. The dual effect of the phonon-phonon couplings in the near-interface region is stemming from the intrinsic wave and quasiparticle-like behaviors of phonons, i.e., these low-frequency phonons can benefit the interfacial thermal transport via phonon interference while the high-frequency phonons hinder the thermal transport via scatterings. For the mechanical-contacted Cu/Si interfaces, we find that the effect of phonon-phonon couplings in the near-interface region can be ignored for the interfacial thermal transport as the contribution from phonon-phonon interference is offset by that from the phonon-phonon scatterings. For the chemical-bonding Cu/Si interfaces, the phonon-phonon couplings in the near interfacial region are found to benefit the interfacial thermal transport at low temperatures (i.e., < 300 K) when the low-frequency phonon-phonon interference is dominant. When the phonon-phonon scatterings become more important at high temperatures (i.e., > 300 K), the phonon-phonon couplings in the near-interface region, therefore, hinder the interfacial thermal transport. Our work here provides a fundamental physical understanding of interfacial thermal transport, considering phonon-phonon couplings across the interface and in the near-interface region.

## 2. Method

### 2.1. Spectral interfacial thermal conductance

The heat current can be calculated as the local energy flux, which is determined by the change of the local Hamiltonian [28], i.e.,

$$Q = \dot{H} \quad (2)$$

in which, the local Hamiltonian  $H = K + U$ , where  $K$  and  $U$  are kinetic and potential energy. We can then write the heat current in the form of

$$Q = \dot{K} + \dot{U} \quad (3)$$

The total potential energy of the system can be written as  $U = \frac{1}{2} \sum_i \sum_{j \neq i} U_{ij}$  where  $U_{ij}$  denotes the pair potential between atoms  $i$  and  $j$ . Therefore, the change rate of the potential energy in Eq. (3) can be calculated as

$$\dot{U} = \frac{1}{2} \sum_i \sum_{j \neq i} \frac{\partial U_{ij}}{\partial \vec{r}_{ij}} \cdot \frac{d\vec{r}_{ij}}{dt} = \frac{1}{2} \sum_i \sum_{j \neq i} \frac{\partial U_{ij}}{\partial \vec{r}_{ij}} \cdot \vec{v}_{ij} \quad (4)$$

in which,  $\vec{r}_{ij} = \vec{r}_j - \vec{r}_i$  is the relative position and  $\vec{v}_{ij} = \vec{v}_j - \vec{v}_i$  is the relative velocity between two atoms. At the same time, the change rate of the kinetic energy in Eq. (3) can be written as

$$\dot{K} = \sum_i m_i \vec{v}_i \cdot \frac{d\vec{v}_i}{dt} = \sum_i \vec{F}_i \cdot \vec{v}_i \quad (5)$$

where  $\vec{F}_i$  and  $\vec{v}_i$  are the atomic force and velocity of atom  $i$ , respectively. In particular, the atomic force  $\vec{F}_i = \sum_{j \neq i} \frac{\partial U_{ij}}{\partial \vec{r}_{ij}}$ , and Eq. (5) is further written as

$$\dot{K} = \sum_i \sum_{j \neq i} \frac{\partial U_{ij}}{\partial \vec{r}_{ij}} \cdot \vec{v}_i \quad (6)$$

For the interfacial heat current, i.e., energy flux across the ideal interface, we introduce the positive sign for the heat current  $Q_{L \rightarrow R}$  from the left contact lead (i.e., denoted as  $L$ ) to the right contact lead (i.e., denoted as  $R$ ). Here, we first assume the interface as an ideal interface with no thickness to separate the atoms into two contact sides. The heat current can then be written in the form of the local energy flux of the left and right contact leads (i.e.,  $Q = \dot{H}_L + \dot{H}_R$ ) [29]. Following Eqs. (4)-(6),

the heat current that arises from the local energy flux of the left and right interfacial sides should also include both the potential energy and kinetic energy terms, and therefore

$$Q = \underbrace{\dot{U}_L + \dot{U}_R}_{Q^{pot}} + \underbrace{\dot{K}_L + \dot{K}_R}_{Q^{kin}} \quad (7)$$

The heat current contributed from the local potential energy  $Q^{pot}$  [Eq. (4)] can then be written as

$$\begin{aligned} Q^{pot} &= Q_L^{pot} + Q_R^{pot} = \dot{U}_L + \dot{U}_R \\ &= \frac{1}{2} \sum_i^L \sum_j^R \frac{\partial U_{ij}}{\partial \vec{r}_{ij}} \cdot \vec{v}_{ij} + \frac{1}{2} \sum_i^L \sum_{i' \neq i}^L \frac{\partial U_{i' i}}{\partial \vec{r}_{i' i}} \cdot \vec{v}_{i' i} \\ &\quad + \frac{1}{2} \sum_j^R \sum_i^L \frac{\partial U_{ji}}{\partial \vec{r}_{ji}} \cdot \vec{v}_{ji} + \frac{1}{2} \sum_j^R \sum_{j' \neq j}^R \frac{\partial U_{j' j}}{\partial \vec{r}_{j' j}} \cdot \vec{v}_{j' j} \end{aligned} \quad (8)$$

and the heat current stemmed from the local kinetic energy  $Q^{kin}$  [Eq. (6)] has the form of

$$\begin{aligned} Q^{kin} &= Q_L^{kin} + Q_R^{kin} = \dot{K}_L + \dot{K}_R \\ &= \sum_i^L \sum_j^R \frac{\partial U_{ij}}{\partial \vec{r}_{ij}} \cdot \vec{v}_i + \sum_i^L \sum_{i' \neq i}^L \frac{\partial U_{i' i}}{\partial \vec{r}_{i' i}} \cdot \vec{v}_i \\ &\quad + \sum_j^R \sum_i^L \frac{\partial U_{ji}}{\partial \vec{r}_{ji}} \cdot \vec{v}_j + \sum_j^R \sum_{j' \neq j}^R \frac{\partial U_{j' j}}{\partial \vec{r}_{j' j}} \cdot \vec{v}_j \end{aligned} \quad (9)$$

As we have defined above, the interfacial heat current across the ideal interface from the left to the right side  $Q_{L \rightarrow R}$  is positive, and therefore, the interfacial heat current contributed from the two sides of the local energy flux has the form of [30]

$$Q_{L \rightarrow R} = \frac{1}{2} (Q_{LR}^{pot} - Q_{RL}^{pot}) + \frac{1}{2} (Q_{LR}^{kin} - Q_{RL}^{kin}) \quad (10)$$

By substituting Eqs. (8) and (9) into Eq. (10), the interfacial heat current is further given by

$$\begin{aligned} Q_{L \rightarrow R} &= \frac{1}{4} \sum_i^L \sum_j^R \left( \frac{\partial U_{ji}}{\partial \vec{r}_{ji}} - \frac{\partial U_{ij}}{\partial \vec{r}_{ij}} \right) \cdot (\vec{v}_i + \vec{v}_j) \\ &\quad - \frac{1}{4} \sum_i^L \sum_{i' \neq i}^L \frac{\partial U_{i' i}}{\partial \vec{r}_{i' i}} \cdot (\vec{v}_i + \vec{v}_i) + \frac{1}{4} \sum_j^R \sum_{j' \neq j}^R \frac{\partial U_{j' j}}{\partial \vec{r}_{j' j}} \cdot (\vec{v}_j + \vec{v}_j) \end{aligned} \quad (11)$$

The first term in Eq. (11) represents the phonon-phonon couplings across the interface, which is usually regarded as the main interfacial thermal transport channel [14,31,29,32,33]. The second and third terms in Eq. (11) are the thermal energy exchange between atoms on the same side, i.e., the phonon-phonon couplings within the same interfacial side, and are thought of as the effect of the near-interface region. These recently developed methods to quantify the spectral thermal transport in the framework of molecular dynamics simulations, such as the spectral heat current (SHC) method [33], interfacial conductance modal analysis (ICMA) [12,34], frequency-dependent directly decomposed method (FDDDM) [14,29,32] and time domain directly decomposed method (TDDDM) [35], all only consider the phonon-phonon couplings across the interfaces. Meanwhile, it has been demonstrated that the interfacial phonon transmission will be affected by the phonon-phonon couplings in the near-interface region [11], i.e., the near-interface effect as denoted. These collisions between localized phonons at the

near-interface region and extended modes can significantly affect the interfacial phonon transmission. In addition, the phonon occupation and the phonon density of the state in the near-interface region are also changed compared to that of the bulk counterpart (Appendix B). It is known that the phonons in molecular dynamics simulations are distributed via equipartition [36]. Therefore, in bulk crystals, each phonon mode has an average energy of  $k_B T$  and a phonon number of  $k_B T / \hbar \omega$  [36]. However, at the near-interface region, the average energy of each phonon mode is different, and therefore, the corresponding phonon occupation number of each phonon mode is changed as well [8]. Therefore, the nonequilibrium distribution of phonons near the interface should be considered when calculating the interfacial thermal transport [37]. It is known that MD simulations inherently include the nature of the nonequilibrium distribution of these phonons near the interface. Our VDOS calculated using regions with various thicknesses near the interface clearly shows that the phonons distribution near the interface is out of the equilibrium distribution (Fig. B1). Meanwhile, the interfacial heat current is calculated using the interatomic partial potentials and velocities of atoms in the interfacial region (see Appendix B for the criteria to determine the interfacial region for details). As a result, our calculated interfacial transmission function in the framework of NEMD simulations inherently includes the nature of the nonequilibrium distribution of these phonons near the interface. However, the phonon distribution in molecular dynamics simulations is an intrinsic property, it is challenging to quantify the influence of the nonequilibrium distribution of phonons near the interface on the interfacial thermal transport.

Based on Eq. (11), we note that the total interfacial heat current is contributed by the phonon-phonon couplings across the interface (i.e., the first term in Eq. (11)) and the phonon-phonon couplings in the near-interface region (i.e., the second and third terms in Eq. (11)). The interfacial heat current contributed by the phonon-phonon couplings in the near-interface region can be written as

$$Q_{L \rightarrow R}^{Near-interface} = -\frac{1}{4} \sum_i^L \sum_{\tilde{i} \neq i}^L \frac{\partial U_{\tilde{i}i}}{\partial \vec{r}_{\tilde{i}i}} \cdot (\vec{v}_i + \vec{v}_{\tilde{i}}) + \frac{1}{4} \sum_j^R \times \sum_{\tilde{j} \neq j}^R \frac{\partial U_{\tilde{j}j}}{\partial \vec{r}_{\tilde{j}j}} \cdot (\vec{v}_j + \vec{v}_{\tilde{j}}) \quad (12)$$

and the heat current resulting from the phonon-phonon couplings across the interface has the form of

$$Q_{L \rightarrow R}^{Across-interface} = \frac{1}{4} \sum_i^L \sum_j^R \left( \frac{\partial U_{ij}}{\partial \vec{r}_{ji}} - \frac{\partial U_{ij}}{\partial \vec{r}_{ij}} \right) \cdot (\vec{v}_i + \vec{v}_j) \quad (13)$$

For the systems depicted by the two-body interactions, such as Lennard-Jones potential, it is known that  $\partial U_{\tilde{i}i} / \partial \vec{r}_{\tilde{i}i} \equiv -\partial U_{i\tilde{i}} / \partial \vec{r}_{i\tilde{i}}$ . Therefore, the interfacial heat current stemming from the phonon-phonon couplings in the near-interface region  $Q_{L \rightarrow R}^{Near-interface}$  becomes zero. The interfacial heat current is identical to the Eq. (13), which can be further written as

$$Q_{L \rightarrow R}^{Across-interface} = -\frac{1}{2} \sum_i^L \sum_j^R \frac{\partial U_{ij}^{two-body}}{\partial \vec{r}_{ij}} \cdot (\vec{v}_i + \vec{v}_j) \quad (14)$$

For the mechanical-contacted Cu/Si interfaces investigated here,

while the interfacial interaction between Si and Cu is described by a two-body potential, the Cu-Cu and Si-Si interactions for the two contacted bulk leads are depicted by many-body potentials. Therefore, the interfacial heat current stemming from the phonon-phonon couplings in the near-interface region  $Q_{L \rightarrow R}^{Near-interface}$  is not zero since  $\partial U_{\tilde{i}i} / \partial \vec{r}_{\tilde{i}i} \neq -\partial U_{i\tilde{i}} / \partial \vec{r}_{i\tilde{i}}$ . It is noted that Eq. (13) is the basis for computing the spectral heat current in the recently developed SHC [33] or FDDDM [14,29,32] method. However, when the systems are described by a many-body interaction such as the Tersoff potential [17], the atomic pair potential  $U_{\tilde{i}i}$  between atoms  $i$  and  $\tilde{i}$  is affected by their environments, e.g., their neighbor atoms [38]. Therefore, the inequality  $\partial U_{\tilde{i}i} / \partial \vec{r}_{\tilde{i}i} \neq -\partial U_{i\tilde{i}} / \partial \vec{r}_{i\tilde{i}}$  for many-body potentials may result in a considerable contribution from the near interface effects  $Q_{L \rightarrow R}^{Near-interface}$ . The heat current owing to phonon-phonon couplings in the near-interface region [Eq. (12)] can be given as

$$Q_{L \rightarrow R}^{Near-interface} = -\frac{1}{4} \sum_i^L \left( \vec{F}_{i \rightarrow \bar{L}_i} + \vec{F}_{\bar{L}_i \rightarrow i} \right) \cdot \vec{v}_i + \frac{1}{4} \sum_j^R \left( \vec{F}_{j \rightarrow \bar{R}_j} + \vec{F}_{\bar{R}_j \rightarrow j} \right) \cdot \vec{v}_j \quad (15)$$

in which,  $\vec{F}_{i \rightarrow \bar{L}_i} = \sum_{\tilde{i}}^{\bar{L}_i} \frac{\partial U_{\tilde{i}i}}{\partial \vec{r}_{\tilde{i}i}}$  denotes the force exerted on the atom  $i$  by atomic groups  $\bar{L}_i$  (i.e., the atoms on the left interfacial side but excluding atom  $i$ ), and  $\vec{F}_{\bar{L}_i \rightarrow i} = \sum_{\tilde{i}}^{\bar{L}_i} \frac{\partial U_{i\tilde{i}}}{\partial \vec{r}_{i\tilde{i}}}$  is the force exerted on atomic groups  $\bar{L}_i$  by atom  $i$ . These forces can be approximated via

$$\vec{F}_{i \rightarrow \bar{L}_i} = \sum_{\tilde{i}}^{\bar{L}_i} \frac{\partial U_{\tilde{i}i}}{\partial \vec{r}_{\tilde{i}i}} \approx \sum_{\tilde{i}}^{\bar{L}_i} \frac{\Delta U_{\tilde{i}i}}{\Delta \vec{r}_{\tilde{i}i}} \Big|_{\Delta \vec{r}_{\tilde{i}i} \rightarrow 0} \quad (16)$$

$$\vec{F}_{\bar{L}_i \rightarrow i} = \sum_{\tilde{i}}^{\bar{L}_i} \frac{\partial U_{i\tilde{i}}}{\partial \vec{r}_{i\tilde{i}}} \approx \sum_{\tilde{i}}^{\bar{L}_i} \frac{\Delta U_{i\tilde{i}}}{\Delta \vec{r}_{i\tilde{i}}} \Big|_{\Delta \vec{r}_{i\tilde{i}} \rightarrow 0} \quad (17)$$

in which  $U_{\tilde{i}i}$  denoted the atomic potential energy between the atoms  $i$  and  $\tilde{i}$ . One can numerically calculate  $\vec{F}_{i \rightarrow \bar{L}_i} = \sum_{\tilde{i}}^{\bar{L}_i} \frac{\partial U_{\tilde{i}i}}{\partial \vec{r}_{\tilde{i}i}}$  using the finite displacement method (FDM). Here, we apply a small displacement  $\Delta \vec{r}_{\tilde{i}i}$  on the atom  $\tilde{i}$ , and then we obtain the corresponding change of potential energy of groups, i.e.,  $\Delta U_{\tilde{i}i}^{\Delta \vec{r}_{\tilde{i}i}} = U_{\tilde{i}i}^{\Delta \vec{r}_{\tilde{i}i}} - U_{\tilde{i}i}^0 = \sum_{\tilde{i}}^{\bar{L}_i} \Delta U_{\tilde{i}i} |_{\Delta \vec{r}_{\tilde{i}i}}$ . The  $\Delta U_{\tilde{i}i}^{\Delta \vec{r}_{\tilde{i}i}}$  is calculated by subtracting the potential energy of groups  $\bar{L}_i$  before the displacement to that after the displacement. The interatomic forces  $\vec{F}_{i \rightarrow \bar{L}_i}$  can then be obtained using Eq. (16). The interatomic forces  $\vec{F}_{\bar{L}_i \rightarrow i}$  can be calculated using the same way. In our calculations, we applied the FDM to calculate all the interatomic forces arising from the many-body interactions. Meanwhile, we also compare the FDM-based heat current with the heat current calculated using the explicit interatomic forces across mechanical-contacted Cu/Si interfaces and find they are the same (Appendix A).

We then apply the spectral heat current decomposition method developed recently [14,29,32,33,39] to both Eqs. (13) and (15). The spectral heat current resulting from the phonon-phonon couplings in the near interface is

and the spectral heat current stemming from the phonon-phonon couplings across the interface is

$$Q_{L \rightarrow R}^{Near-interface}(\omega) = \frac{1}{2} \sum_j^R \text{Re} \left[ \int_{-\infty}^{+\infty} \left\langle \left[ \vec{F}_{j \rightarrow \bar{R}_j}(\tau) + \vec{F}_{\bar{R}_j \rightarrow j}(\tau) \right] \Big|_{\tau} \cdot \vec{v}_j(0) \right\rangle e^{-i\omega\tau} d\tau \right] \text{nonumber} \quad (18)$$

$$- \frac{1}{2} \sum_i^L \text{Re} \left[ \int_{-\infty}^{+\infty} \left\langle \left[ \vec{F}_{i \rightarrow \bar{L}_i}(\tau) + \vec{F}_{\bar{L}_i \rightarrow i}(\tau) \right] \Big|_{\tau} \cdot \vec{v}_i(0) \right\rangle e^{-i\omega\tau} d\tau \right]$$

$$Q_{L \rightarrow R}^{\text{Across-interface}}(\omega) = \frac{1}{2} \sum_i^L \sum_j^R \text{Re} \left[ \int_{-\infty}^{+\infty} \left\langle \left[ \frac{\partial U_{ji}}{\partial \vec{r}_{ji}}(\tau) - \frac{\partial U_{ij}}{\partial \vec{r}_{ij}}(\tau) \right] \cdot \left[ \vec{v}_i(0) + \vec{v}_j(0) \right] e^{-i\omega\tau} d\tau \right\rangle \right] \quad (19)$$

in which,  $\tau$  is the correlation time and  $\langle \rangle$  denotes time average in MD simulations. By considering the phonon-phonon couplings in the near-interface region and across the interface, the spectral interfacial heat current in the NEMD simulations can then be calculated via

$$Q_{L \rightarrow R}^{\text{Total}}(\omega) = Q_{L \rightarrow R}^{\text{Across-interface}}(\omega) + Q_{L \rightarrow R}^{\text{Near-interface}}(\omega) \quad (20)$$

By assuming the same interfacial temperature drop on all the phonons, the spectral ITC can be evaluated via Fourier's law [40]

$$G(\omega) = Q_{L \rightarrow R}^{\text{Total}}(\omega) / A \Delta T \quad (21)$$

where  $A$  is the cross-sectional area and  $\Delta T$  denotes the temperature drop at the ideal interface. The temperature drop used to calculate the ITC is obtained at the ideal interface by linearly fitting the temperature profiles of two contact leads. Therefore, the ITC spectrums resulting from the phonon-phonon couplings across the ideal interface and in the near interfacial region can be characterized as

$$G^{\text{Across-interface}}(\omega) = Q_{L \rightarrow R}^{\text{Across-interface}}(\omega) / A \Delta T \quad (22)$$

and

$$G^{\text{Near-interface}}(\omega) = Q_{L \rightarrow R}^{\text{Near-interface}}(\omega) / A \Delta T \quad (23)$$

respectively.

## 2.2. Spatial phonon interference characterization

To determine the influence of phonon-phonon couplings in the near-interface region on interfacial thermal transport, we calculate the spatial phonon-phonon interference in the near-interface region. As suggested by Latour *et al.* [27], the spatial phonon-phonon interference corresponds to the spatial correlations between the atomic displacement fluctuations at equilibrium positions, i.e., the motions of two atoms are correlated when they oscillate with a given phase relationship. We can then calculate the mutual interference function [27] between two transverse planes of coordinates  $z_m$  and  $z_n$  along the correlation direction  $\vec{e}_{\parallel}$  through

$$\Gamma(z_m, z_n, \tau) = \frac{1}{k_B T N_{\perp}} \sum_i^{N_c} \sum_j^{N_c} \sum_{\gamma}^{N_b} \sqrt{m_i^{\gamma} m_j^{\gamma}} \left\langle \vec{v} \left( \vec{r}_i^{0\gamma}, t \right) \vec{v} \left( \vec{r}_j^{0\gamma}, t + \tau \right) \right\rangle \cdot \delta \left[ \left( \vec{r}_i^0 - \vec{r}_j^0 \right) \cdot \vec{e}_{\perp 1} \right] \delta \left[ \left( \vec{r}_i^0 - \vec{r}_j^0 \right) \cdot \vec{e}_{\perp 2} \right] \delta \left[ \vec{r}_i^0 \cdot \vec{e}_{\parallel} - z_m \right] \delta \left[ \left( \vec{r}_j^0 \cdot \vec{e}_{\parallel} - z_n \right) \right] \quad (24)$$

in which,  $N_c$  is the total number of cells in the system,  $N_b$  is the number of atoms in the unit cell,  $N_{\parallel}$  is the number of cells along the direction  $\vec{e}_{\parallel}$ ,  $N_{\perp}$  is the number of cells in the orthogonal plane to  $\vec{e}_{\parallel}$ , i.e., along the directions of  $\vec{e}_{\perp 1}$  and  $\vec{e}_{\perp 2}$ ,  $m_i^{\gamma}$  is the mass of atom  $\gamma$  in the cell  $i$ ,  $k_B$  is the Boltzmann constant,  $\delta[x]$  is the Dirac function, and  $T$  is the temperature. The atomic positions are decomposed as  $\vec{r}_i^{0\gamma} = \vec{r}_i^0 + \vec{r}^{\gamma}$  in which  $\vec{r}_i^0$  is the equilibrium position of the cell  $i$  and  $\vec{r}^{\gamma}$  is the position of the atom  $\gamma$  within the cell. By applying the Fourier transform on Eq. (24), we can calculate the two-point cross-spectral density function  $W(z_m, z_n, \omega)$ , which contains the space-dependent correlation along the direction  $\vec{e}_{\parallel}$ . The degree of interference  $\mu(z_m, z_n, \omega)$  can be then calculated from the

two-point cross-correlation function

$$\mu(z_m, z_n, \omega) = \frac{W(z_m, z_n, \omega)}{[W(z_m, z_m, \omega)]^{1/2} [W(z_n, z_n, \omega)]^{1/2}} \quad (25)$$

where  $W(z_m, z_m, \omega)$  corresponds to the local vibrational density of states (VDOS) of atoms at the position of  $z_m$ . By summing all the possible pairs of planes ( $z_m, z_n$ ), the spatial cross-correlation function is given by [27]

$$C(k\Delta z, \omega) = \frac{1}{N_{\parallel} - 1} \sum_{i=1}^{N_{\parallel}-k} \mu(z_i, z_{i+k-1}, \omega) \quad (26)$$

where  $\Delta z$  denotes the spatial resolution of the correlation, and  $k \in \{0 \dots N_{\parallel} - 1\}$ . Using Eq. (26), we can then characterize the degree of phonon-phonon interference in the near-interface region.

## 2.3. Simulation setup

Two typical systems, i.e., mechanical-contacted and chemical-bonding Cu/Si interfaces, are chosen to investigate the influence of phonon-phonon couplings in the near-interface region on the interfacial thermal transport using non-equilibrium molecular dynamics (NEMD) simulations. The interactions for Cu-Cu and Si-Si are depicted by many-body potentials [17,41]. The interactions between Cu and Si are described by either a two-body potential or a many-body potential, which represents two typical types (i.e., mechanical contact and chemical bond) of interfaces in realistic. We demonstrate that the near-interface effect generally exists in all interfaces. Therefore, we choose Cu/Si interfaces as our research objects here. All the MD simulations were performed using the LAMMPS package [42]. The interatomic interactions among mechanical-contacted Cu and Si atoms are modeled by the Lennard-Jones (LJ) potential [15,16], i.e.,  $U(r) = 4\epsilon \left[ (\sigma/r)^{12} - (\sigma/r)^6 \right]$  with the parameter  $\epsilon = 0.030999\text{eV}$  and  $\sigma = 3.0\text{\AA}$ . Here,  $r$  denotes the atomic distance, and the cut-off distance for the LJ potential is  $2.5\sigma$ . It is known that the LJ potential is widely used for describing the van der Waals interaction between atoms [15], which therefore can mimic the mechanical contact interfaces in experiments [16]. The chemical-bonded interfaces such as Si/SiC [43] and GaN/SiC [44] interfaces in experiments can be depicted by many-body potentials (i.e., the Tersoff potential here) [17,45]. As we mentioned above, we apply the LJ potential and Tersoff potential to mimic the interactions of two typical types of interfaces, i.e., mechanical-contacted and chemical-bonded interfaces, respectively. The interatomic interaction for chemical-bonding Cu-Si is depicted by the Tersoff potential [18]. The embedded atomic method (EAM) potential [41] and the Tersoff potential [17] are applied to describe Cu-Cu interactions and Si-Si interactions, respectively. It is known that heterointerfaces can be formed via physical bonding such as van der Waals stacking [46,47], in which the interfacial bonds are weak and can be described by two-body potentials. Meanwhile, it is also popular to apply chemical methods such as molecular beam epitaxy growth to fabricate heterointerfaces [48] of which the interfacial bonds are strong and depicted by many-body potentials.

The simulation timestep is 0.5 fs for our simulations. The lattice constants are 5.4305Å for Si and 3.6150Å for Cu, respectively. The Si and Cu sides are connected at the [111] lattice orientation. The lengths of the Si and Cu sides are 44 nm ( $L_x^{\text{Si}} = 44\text{nm}$ ) and 54 nm ( $L_x^{\text{Cu}} = 54\text{nm}$ ),

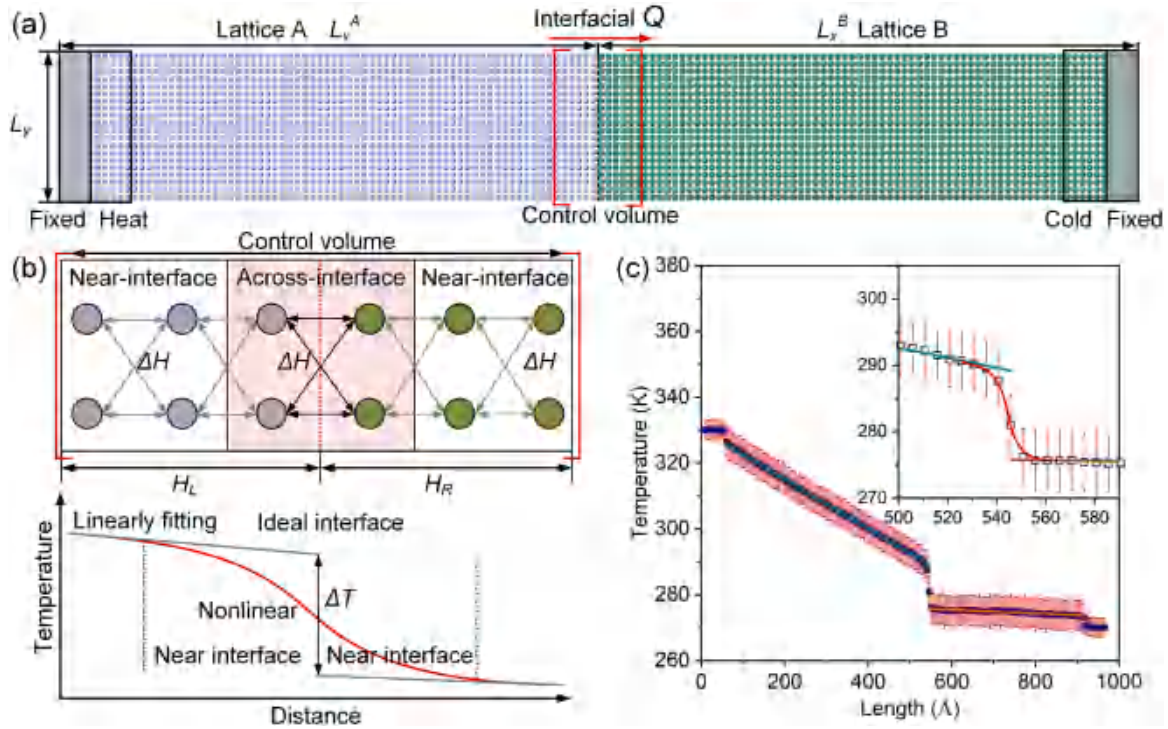


**Fig. 2.** (a) The NEMD simulation model of Cu/Si systems. The Si lead with a length of 44 nm ( $L_v^{\text{Si}} = 44\text{nm}$ ) is contacted with the Cu lead ( $L_v^{\text{Cu}} = 54\text{nm}$ ), and the cross-section is  $5.34 \times 5.39 \text{ nm}^2$ . (b) The control volume or the interfacial region included the near-interface region and the nonlinear discontinuity of the temperature profile at the near-interface region. (c) A typical temperature profile for a Cu/Si interface at 300 K. The nonlinear discontinuity of the temperature profile extends  $\sim 20 \text{ \AA}$  from the ideal interface.

with the system cross-section of  $5.34 \times 5.39 \text{ nm}^2$ . Periodic boundary conditions are applied to the lateral directions in all our MD simulations.

Before NEMD simulations, the systems are first relaxed in an *NPT* (particle, pressure, and temperature) ensemble for 2 ns to eliminate the residual stress caused by the lattice mismatch and temperature and then changed to an *NVT* (particle, volume, and temperature) ensemble for another 2 ns. Two ends of the systems are fixed during the NEMD simulations, as shown in Fig. 2a. Five layers of atoms closing to the fixed regions with a thickness of 1.0 nm are coupled with Langevin thermostats and selected as the heat source and sink, respectively. We then run NEMD simulations for 8 ns to obtain the stable heat current and temperature distribution. Another 1 ns NEMD simulation is used to extract the atomic potential partial function  $\partial U_{ij}/\partial \vec{r}_{ij}$  and atomic velocity  $\vec{v}_i$ , which are the original inputs for our spectral heat current analysis. For the mechanical-contacted Cu/Si interface described using LJ potential, the atomic potential partial function in across-interface effects [Eq. (19)] can be simplified to the interatomic forces, i.e.,  $\vec{F}_{ij} = \partial U_{ij}/\partial \vec{r}_{ij}$ , which are directly calculated based on the atomic positions. However, for the near-interface effects and the across-interface of chemical-bonding Cu/Si systems, the atomic potential partial function (e.g., [Eq. (12)]) is determined by their neighbor atoms because of the many-body interactions used in our simulations, and we compute them numerically. Here, we apply a two-step MD simulation to obtain the atomic potential partial function involving the many-body interactions. We first output the time-dependent atomic configurations together with the atomic velocity of the interfacial region during the NEMD simulations. The dumped atomic configurations are then used as data files for the next sets of static calculations to compute the interfacial atomic forces. Here, we calculate the partial potential functions based on the FDM [Eq. (15)], which inherently considers all many-body interactions (See details and validations in Appendix A).

Meanwhile, the atomic potential partial function and atomic velocity

of the interfacial region with a size of  $\sim 2.2 \text{ nm}$  for Cu/Si are collected every ten timesteps. While previous studies [32,35] showed that the interfacial region used here may be large enough to obtain a converged interfacial heat current spectrum, they only considered the phonon-phonon couplings across the interface in their results. As phonon-phonon couplings across the interface and in the near interfacial region [Eq. (11)] are included in our calculations, we recheck the size effect of the interfacial region on our calculated results. The interfacial region is defined as where we calculate the interfacial heat current using Eqs. (11)-(13), (18)-(19), which can be understood as the near-interface region where phonon-phonon couplings are significantly different from that inside its bulk counterparts. Therefore, the interfacial region should be large enough to include the near-interface effect [32]. Here, we determine the size of the interfacial region based on the spectral heat current (Appendix B) and VDOS (Appendix B). Our results show that the interfacial region in our simulations is large enough to include the near-interface effect (Appendix B). We also emphasize that the interfacial region fully covers the nonlinear temperature distribution region (the nonlinear temperature distribution region is  $\sim 20 \text{ \AA}$  for Cu/Si interface, Figs. 2b and 2c) of the systems. It is noted that the nonlinear discontinuity in the temperature profile is not caused by the atomistic disorder near the interface [49] since the atoms in the near interfacial region vibrate at the lattice sites. The nonlinear effect in temperature distribution should result from the interface region's inherent nature, i.e., the phonons near the interface should be highly non-equilibrium due to the reflection and transmission occurring at the interface [50]. Correspondingly, phonon-phonon couplings at the near interfacial region could largely deviate from that in bulk, which may essentially affect the interfacial thermal transport [50]. As discussed above, the phonon-phonon couplings (Fig. 2b) at the near-interface region can be quantified using the second and third terms in Eq. (11).

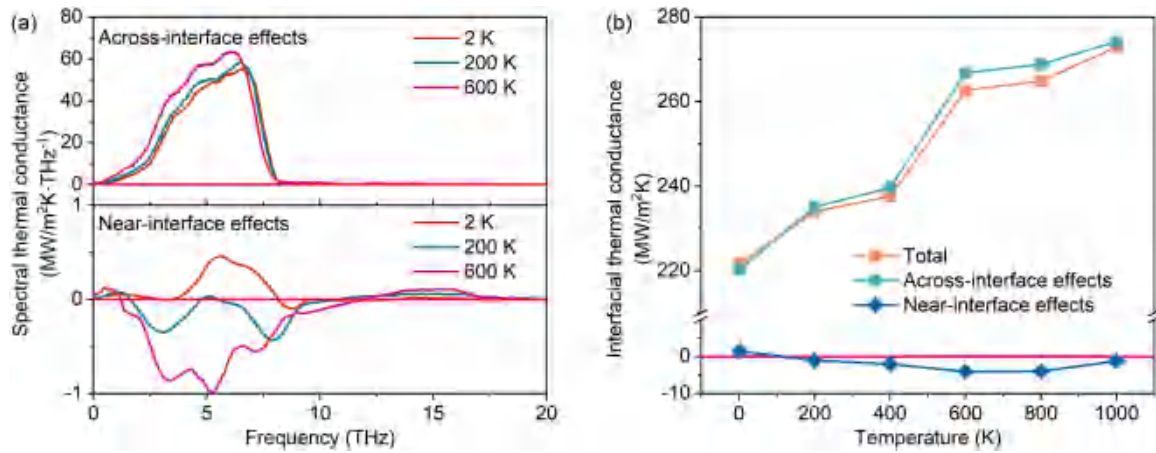


**Fig. 3.** (a) The spectral interfacial thermal conductance and (b) the corresponding accumulative thermal conductance of mechanical-contacted Cu/Si interfaces at temperatures ranging from  $T = 2$  K to  $T = 1000$  K. The spectral thermal conductance resulted from the phonon-phonon couplings across the interface and in the near-interface region are calculated using Eq. (22) and (23), respectively.

### 3. Result and discussion

#### 3.1. Mechanical-contacted Cu/Si interfaces

We first investigate thermal transport across the mechanical-contacted Cu/Si interfaces at various temperatures (i.e., from 2 K to 1000 K), considering phonon-phonon couplings across the interface and in the near-interface region. It is noted that the electron-phonon couplings are ignored here as phonons are the dominant heat carriers for thermal transport across Cu/Si interfaces [51]. At the same time, while the interfacial interaction for mechanical contact interfaces is depicted using a two-body potential, the two contacted leads are described by many-body potentials. The near-interface effect will then affect the interfacial thermal transport as we discussed above.

We find that the ITC is mainly contributed by phonon-phonon couplings across the interfaces at temperatures ranging from 2 K to 1000 K (Figs. 3a and 3b). This is because the nonlinear effect in the near-interface region is weak for the mechanical-contacted Cu/Si interfaces. However, it should be noted that the near-interface effect on the interfacial thermal transport is small while indeed exists in the mechanical-contacted Cu/Si systems (Fig. 3b). More interesting, the phonon-phonon couplings in the near-interface region are found to contribute to the interfacial thermal transport from two aspects: 1) these low-frequency phonons (e.g.,  $< \sim 2$  THz as shown in Fig. 3a) will benefit the interfacial thermal transport and 2) the high-frequency phonons (e.g.,  $> 2$  THz as shown in Fig. 3a) will suppress the interfacial thermal transport. As shown in Eq. (11), phonon-phonon couplings occur in the near-interface region and do not transport thermal energy from one side to another. Then, a question can be easily raised: how do the phonon-phonon couplings in the near-interface region contribute to interfacial thermal transport?

On the one hand, the thermal energy exchange across the interface between two contacted leads includes both elastic and inelastic phonon-phonon couplings across the interfaces [14,16,32,33,37]. More inelastic phonon-phonon couplings across the interfaces are activated and, therefore, benefit the interfacial thermal transport, which leads to the increase of the ITC with temperatures even when all the phonons are occupied (Figs. 3a and 3b). On the other hand, a phonon is the quantum description of an elementary vibration in which a lattice of atoms uniformly oscillates at a single frequency [49,52] and, therefore, should be an intrinsic wave. Meanwhile, it is popular to treat phonons as quasiparticles and investigate the corresponding thermal transport properties based on the "phonon-gas" model [53,54]. Here, we explain and discuss the phonon scattering picture by regarding phonons as quasiparticles. As the phonons are intrinsic waves, they possess wave behaviors (e.g.,

interference) [25,55]. In classical MD simulations, the scatterings and the interference among phonons are inherently included [22,23], and the interference among phonons can even be directly observed in the MD simulations [56]. At the same time, it has been demonstrated that the extended phonon modes are strongly affected by the localized phonons in the near-interface region [11,37], and the phonon-phonon couplings between them are found to affect the total interfacial phonon transmission [9,12]. These high-frequency or equivalently short-wavelength phonons in the near-interface region can be well-treated as quasiparticles and collide with these extended phonon modes. Therefore, the heat current spectrum of these extended phonon modes decreases when the scatterings between these extended phonon modes and these high-frequency localized phonons are considered. Meanwhile, the wave behavior of these low-frequency or equivalently long-wavelength phonons (e.g., phonon-phonon interference) is found to be important in many systems [22,23,57]. Therefore, these low-frequency or equivalently long-wavelength phonons in the near-interface region can interfere with these extended phonon modes. The interference between these low-frequency phonon modes and the extended phonon modes will benefit the propagation of the extended phonon modes [22]. As a result, the spectrum of the heat current of these

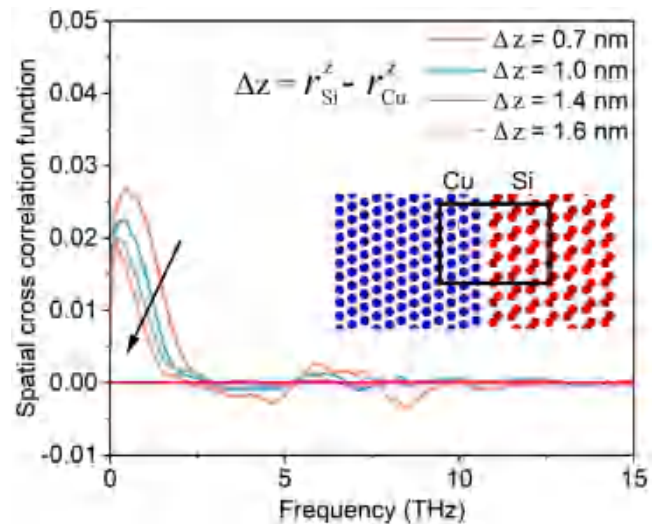


**Fig. 4.** The spatial cross-correlation functions [Eq. (26)] at the near-interface regions of mechanical-contacted Cu/Si interfaces for vibrations transverse between Cu and Si leads. All the results are calculated at  $T = 2$  K.

extended phonon modes increases when the interference between these extended phonon modes and these low-frequency localized phonons is considered.

We further calculate the spatial cross-correlation function [Eq. (26)] of the interfacial region, which has successfully been used to characterize phonon-phonon interference [27,58]. The larger spatial cross-correlation value indicates stronger phonon-phonon interference, as demonstrated by Latour *et al.* [27]. Here, we first map the interfacial atoms of the Cu/Si system within a superlattice structure in which three Cu unit cells are coupled with two Si unit cells in the orthogonal directions (Fig. 4). The atomic pairs  $(i,j)$  satisfied  $(r_i^x - r_j^x)^2 + (r_i^y - r_j^y)^2 \leq 0.0001 \text{ \AA}^2$  are selected to calculate the spatial cross-correlation function [Eq. (26)]. Our results show that the interference among these low-frequency phonons (i.e.,  $< 2$  THz) at the interface region is strong (Fig. 4) and therefore benefits the interfacial thermal transport (Fig. 3a). The interference among these high-frequency phonons (i.e.,  $> 5$  THz) can be ignored (Fig. 4), and the high-frequency phonons behave like scatters and will suppress the interfacial thermal transport (Fig. 3a). This is because low-frequency phonons have long wavelengths, and therefore their wave nature should be considered when calculating thermal transport properties. However, the wavelengths of high-frequency phonons are short and can be regarded as quasiparticles. It is also noted that phonon-phonon interference (phonon-phonon scatterings) becomes stronger when the temperature increases (see Appendix D), which stems from the larger overlap of phonon linewidth (increasing anharmonicity) [59].

We emphasize that it is quite challenging to directly capture the phonon-phonon scattering or interference process in MD simulations. Our work here focuses on quantifying the near-interface effects on interfacial thermal transport. It has been demonstrated that inelastic phonon-phonon scatterings in the near-interfacial region can hinder interfacial thermal transport [50]. Therefore, the interfacial spectral heat current should decrease when inelastic phonon-phonon scatterings in the near-interfacial region are included. However, our work here shows that the phonon-phonon interference in the near-interfacial region can facilitate interfacial thermal transport. At an extremely low temperature of 2 K, inelastic phonon-phonon scatterings can be ignored. Our results show that the heat current spectrum resulting from the near-interfacial effect is positive (i.e., benefiting the interfacial thermal transport), which directly demonstrates that the near-interfacial effect can benefit the interfacial thermal transport. We further calculate the spatial correlation function of phonons which can be used to

phenomenologically demonstrate the interference between phonons caused by their wave nature [27] (Appendix D). Our results show that the spatial cross-correlation function of these low- and middle-frequency phonons is large, which implies there exists interference or coherence among these phonons. It is believed that the facilitation of interfacial thermal transport from the near-interfacial effect is caused by the interference or coherence among these phonons.

### 3.2. Chemical-bonding Cu/Si interfaces

We then studied the influence of phonon-phonon couplings in the near-interface region on thermal transport across the chemical-bonding Cu/Si interface. As we did for the mechanical-contacted Cu/Si interfaces above, we quantify the phonon-phonon couplings across the chemical-bonding Cu/Si interface [Eq. (19)] and in the near-interface region [Eq. (18)]. It is known that the phonon-phonon couplings across the interface contribute to interfacial thermal transport via harmonic processes at extremely low temperatures [14,16,29]. Here, the Debye temperatures for Cu and Si are 343 K [60] and 645 K [60], respectively. Our results show that only these phonons with frequencies smaller than 8.0 THz (i.e., the cut-off frequency for Cu) contribute to the interfacial thermal transport via harmonic processes (Fig. 5a) at 2 K. At this temperature, the phonon-phonon couplings in the near-interface region contribute to the interfacial thermal transport through interference. The quasiparticle-like behavior of phonons (i.e., phonon-phonon scatterings in the near-interface region) can almost be ignored at the temperature of 2 K. When the temperature increases to 100 K, phonon-phonon scatterings in the near-interface region become stronger and will hinder the interfacial thermal transport (Fig. 5b). As we discussed above, both interference and scatterings among phonons will become stronger when the temperature increases. When the system temperature is higher than 300 K (Figs. 6a and 6b), the scatterings overwhelm the interference among these phonons with frequencies higher than 5 THz. As a result, the scatterings among these phonons (i.e.,  $> 5$  THz) in the near-interface region will hinder the interfacial thermal transport. For these phonons with frequencies lower than 5 THz, we find that the interference overwhelms the scattering among these phonons. Consequently, the couplings among these phonons in the near-interface region benefit the interfacial thermal transport through interference.

We also calculate the spatial cross-correlation function for the Cu/Si systems using Eqs. (24)-(26). Our results show that the spatial cross-correlation function of the phonons with frequencies smaller than 2.5 THz in the Cu/Si interfacial region is strong (Fig. 7), which indicates a

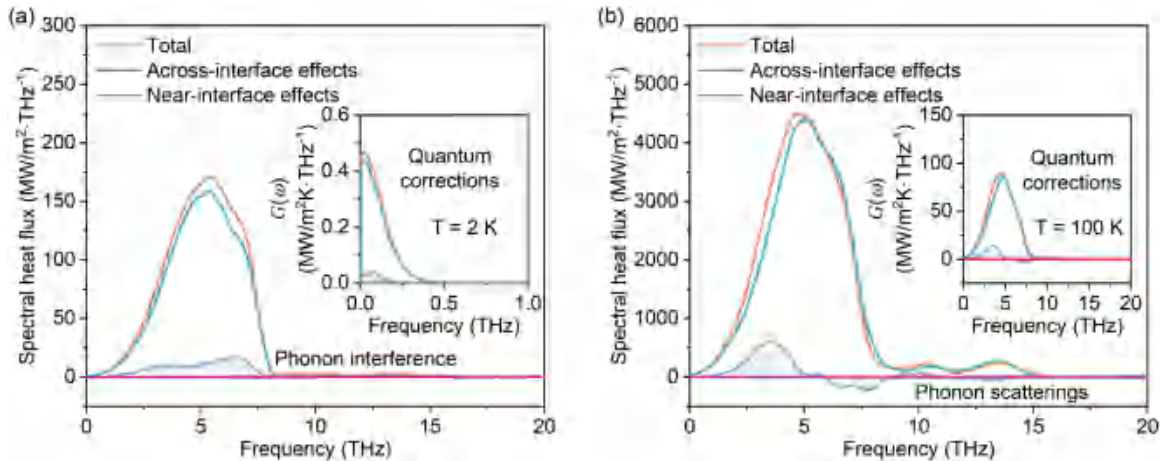


Fig. 5. The spectral interfacial heat fluxes across chemical-bonding Cu/Si interfaces at (a)  $T = 2$  K and (b)  $T = 100$  K. The spectral heat fluxes resulted from the phonon-phonon couplings across the interface and in the near-interface region are calculated using Eqs. (18) and (19). The insets are the corrected spectral interfacial thermal conductance calculated based on Landauer theory [62], in which we integrate the Bose-Einstein distribution with the phonon transmission function calculated from NEMD simulations, i.e.,  $G_{QC} = \frac{1}{2\pi A} \int_0^\infty \hbar\omega \frac{\partial f(\omega, T)}{\partial T} \Gamma(\omega, T) d\omega$ .

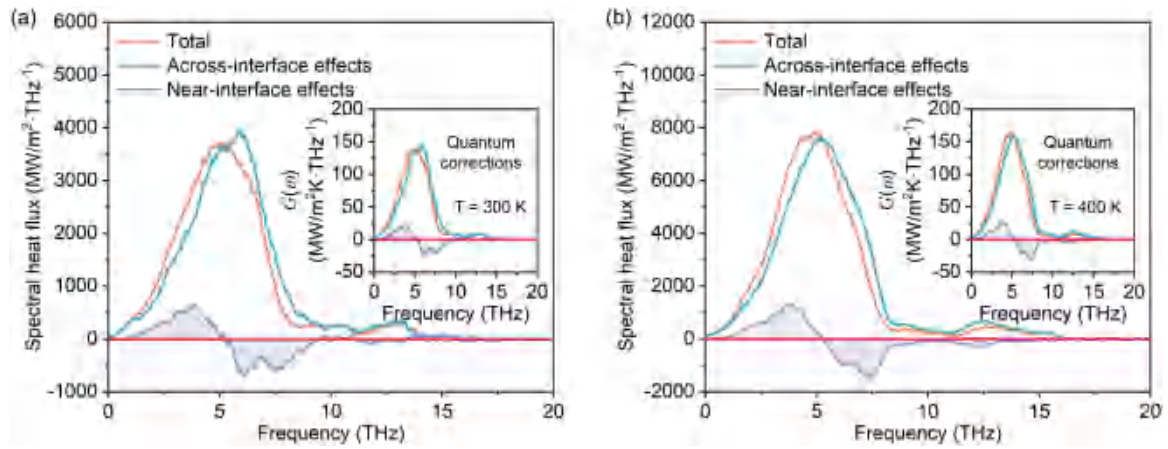


Fig. 6. The spectral interfacial heat fluxes across chemical-bonding Cu/Si interfaces at (a)  $T = 300$  K and (b)  $T = 400$  K. The calculation detail is the same to that in Fig. 5.

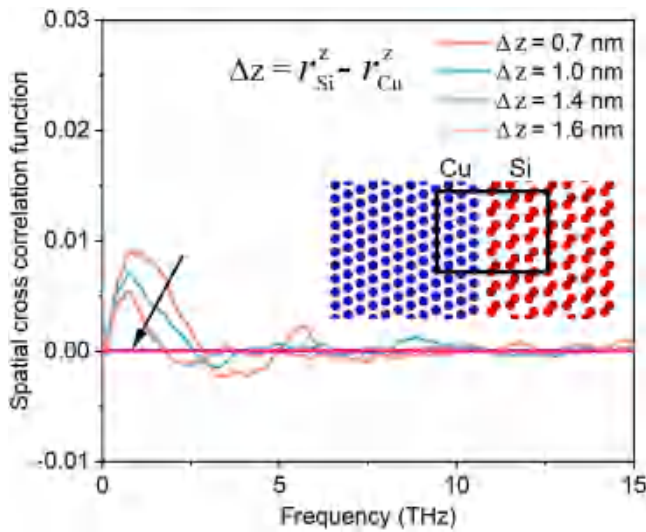


Fig. 7. The spatial cross-correlation functions at the near-interface regions for vibrations transverse between Cu and Si leads of chemical-bonding Cu/Si interface. All the results here are calculated at  $T = 2$  K.

strong interference among these phonons. For instance, the phonon cross-correlation function for a traveling distance of 1.6 nm, which is comparable to the length of the interfacial region, is still considerable for the chemical-bonding Cu/Si interface. Therefore, the strong phonon cross-correlation between Cu and Si largely benefits the interfacial thermal transport, as we have observed in Fig. 5a.

It should be noted that all the phonons are fully occupied in molecular dynamics simulations, which is only valid when the temperature is well above the Debye temperature [61]. The quantum correction should be applied to our calculated interfacial thermal transport properties to mitigate this. In NEMD simulations, the phonon transmission coefficient can be calculated via  $\Gamma(\omega, T) = Q(\omega, T)/k_B\Delta T$  (Appendix C) [62]. The interfacial thermal conductance can then be corrected quantumly via  $G_{QC} = \frac{1}{2\pi A} \int_0^\infty \hbar\omega \frac{\partial f(\omega, T)}{\partial T} \Gamma(\omega, T) d\omega$  [62], in which  $f(\omega, T)$  is the phonon distribution function following the Bose-Einstein distribution. Our results show that the spectral ITC is largely changed at low temperatures (i.e., 2 K and 100 K as shown in Fig. 5) since only these low-frequency phonons are occupied at low temperatures. However, the phonon-phonon couplings in the near-interface region will affect the interfacial thermal transport via interference at low temperatures (Fig. 5). Furthermore, the high-frequency phonons are occupied when

the temperature increases to 300 K, and their scatterings are included in the near-interface effects (Fig. 6). Therefore, our conclusions (i.e., phonon-phonon couplings in the near-interface affect the interfacial thermal transport via interference and scatterings) will not be changed by the quantum correction (Figs. 5 and 6).

### 3.3. Competition between phonon-phonon interference and phonon-phonon scattering

As discussed above, phonon-phonon couplings in the near-interface region have dual effects on interfacial thermal transport owing to the intrinsic wave and quasiparticle-like behaviors of phonons. We find that the phonon-phonon couplings among these low-frequency phonons in the near-interface region can benefit the interfacial thermal transport via interference, and the phonon-phonon couplings among the high-frequency phonons in the near-interface region hinder the interfacial thermal transport through scatterings. As a result, the influence of the phonon-phonon couplings in the near-interface region on the interfacial thermal transport is resulting from the competition between these two effects.

For the mechanical-contacted Cu/Si interfaces, without considering the quantum effect in our results, we find that the influence of phonon-phonon couplings in the near-interface region on the interfacial thermal transport could be negligible (Figs. 3a and 3b). The ITC only needs to consider the phonon-phonon couplings across the interface. This is because the positive effect on interfacial thermal transport via the interference among the phonons in the near-interface region is largely offset by the negative effect through scatterings among these phonons.

We next investigate the influence of phonon-phonon couplings in the near-interface region on the thermal transport of chemical-bonding Cu/Si interfaces. Unlike the mechanical-contacted interfaces, phonon-phonon couplings across and in the near-interface region of chemical-bonding Cu/Si interfaces are found to contribute non-negligible to interfacial thermal transfer when all the phonons are fully occupied, which is inherently assumed in MD simulations. For instance, at a low temperature of 2 K, the phonon-phonon couplings across the interface contribute around 90 % to the ITC, while the remaining 10 % of the ITC results from the phonon-phonon couplings in the near-interface region through interference (Figs. 8a and 8b). As mentioned above, the phonon-phonon couplings in the near-interface region affect the interfacial thermal transport through phonon-phonon interference or phonon-phonon scattering. Therefore, the phonon-phonon couplings in the near-interface region have a positive effect on the interfacial thermal transport when the phonon-phonon interference overcomes the phonon-phonon scattering (e.g.,  $< 300$  K for the chemical-bonding Cu/Si interfaces). If phonon-phonon scatterings in the near-interface region are

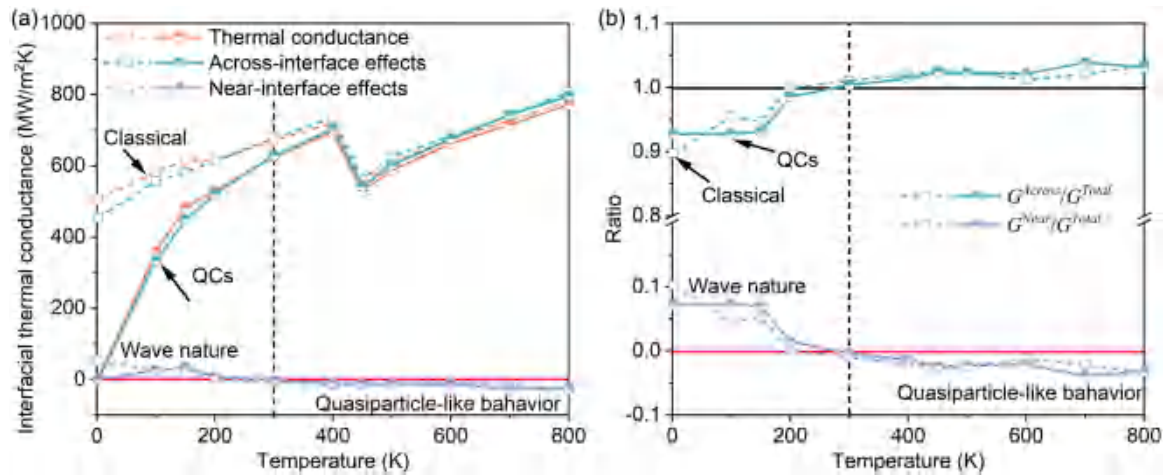


**Fig. 8.** (a) The interfacial thermal conductance of Cu/Si interfaces resulted from phonon-phonon couplings across the interface and in the near-interface region calculated using Eqs. (21)–(23) (dashed lines represent classical results, and solid lines are the corrected results). (b) The contributions resulted from phonon-phonon couplings across the interface and in the near-interface region to the total interfacial thermal conductance. The interfacial thermal conductance drop at 430 K is caused by the mixing of interfacial atomic layers between Si and Cu. We also apply quantum corrections to all the results (labeled by QCs, solid lines) based on the Landauer transport theory [62], and the calculation details can be found in Section 3.2.

dominant, phonon-phonon couplings in the near-interface region will have a negative influence on the interfacial thermal transport (e.g., > 300 K for the Cu/Si interfaces). It should be noted that at high temperatures above 300 K, the interference among these low-frequency phonons in the near-interface region also exists, but their contribution to the interfacial thermal transport is offset and even overwhelmed by the scatterings among the high-frequency phonons. The sudden drop of interfacial thermal conductance of Cu/Si interfaces at ~450 K is caused by the phase change of atoms in the interfacial region, which stems from the mixture of atomic layers due to the increasing temperature (Fig. 8a).

Next, we also perform the quantum corrections to the ITC of Cu/Si interfaces. While the quantum correction changes the ITC (Fig. 8a), the phonon-phonon couplings in the near-interface region still affect the interfacial thermal transport via the competition between phonon interference and phonon scatterings (Fig. 8b). At low temperatures (e.g.,  $T < 200$  K), the low-frequency phonons (< 5 THz) are mostly activated and will benefit the interfacial thermal transport through the interference among these phonons in the near-interface region. However, the phonons with frequencies higher than 5 THz do not occupy and therefore affect the interfacial thermal transport a little. Therefore, the phonon-phonon couplings will mainly benefit the interfacial thermal transport across Cu/Si interfaces through interference at low temperatures (e.g., the phonon-phonon couplings in the near-interface region can contribute ~10 % to ITC at 2 K as shown in Fig. 8b). When the temperature is higher than 300 K, high-frequency phonons are gradually occupied, the phonon-phonon couplings will hinder the interfacial thermal transport through scatterings. We further show that our results considering quantum corrections will converge to the results of classical MD (Fig. 8a) when the temperature is higher than 400 K when all the phonons with frequencies smaller than 8 THz (i.e., the cut-off frequency of Cu) are fully occupied.

#### 4. Consistent with the second law of thermodynamics

We would like to emphasize that the heat current [Eq. (11)] and the heat current spectrum [Eq. (20)], which considers both phonon-phonon couplings across the interface and in the near-interface region are positive based on the second law of thermodynamics. It is known that the heat current of a specific vibrational mode across the interface will decrease when this vibrational mode is scattered by other vibrations in the near interfacial region [63]. As we discussed before, the heat current spectrum only considering phonon-phonon couplings in the

near-interface region (i.e., second and third terms in Eq. (11)) will affect the interfacial thermal transport from two aspects: benefit the interfacial thermal transport via phonon interference caused by the wave nature of phonons (i.e., increase the heat current of these involved vibrational modes) and hinder the interfacial thermal energy transfer through scatterings stemmed from the quasiparticle-like behavior of phonons (i.e., decrease the heat current of these involved vibrational modes). At extremely low temperatures, e.g., 2 K for the Cu/Si systems, the scatterings among phonons can be ignored, and therefore, the heat current spectrum only considering phonon-phonon couplings in the near-interface region should be larger than zero, as demonstrated in our calculations (Figs. 3 and 5). When the temperature increases, the scatterings among phonons are activated, which then hinders the interfacial thermal energy transfer of these vibrational modes. Consequently, the heat current at high temperatures, only considering phonon-phonon couplings in the near interfacial region, is decreasing compared to 2 K. The heat current resulting from the phonon-phonon couplings in the near-interface region can be even smaller than zero when phonon-phonon scatterings play a more important role than the phonon-phonon interference in the near-interface region (Figs. 3 and 8).

#### 5. Conclusion

In conclusion, we have revisited the interfacial thermal transport by considering phonon-phonon coupling across the interface and in the near-interface region. By calculating the spectral interfacial heat current in the framework of NEMD simulations, we demonstrate that the phonon-phonon couplings in the near-interface region have a dual influence on the interfacial thermal transport which is resulting from the intrinsic wave and quasiparticle-like behaviors of phonons. On the one hand, the interference among these low-frequency phonons in the near-interface region can benefit interfacial thermal transport. On the other hand, phonon-phonon couplings between these high-frequency phonons in the near-interface region will hinder interfacial thermal transport via scatterings. Two typical systems (i.e., mechanical-contacted and chemical-bonding Cu/Si interfaces) are then chosen as examples to investigate the interfacial thermal transport considering phonon-phonon couplings across the interface and in the near-interface region. For mechanical-contacted Cu/Si interfaces, the contribution from the phonon-phonon couplings in the near-interface via interference is mainly offset by that through scatterings. Therefore, the interfacial thermal transport is dominant by the phonon-phonon couplings across

the interface. For chemical-bonding Cu/Si interfaces, we find the phonon-phonon couplings in the near-interface region contribute as high as 10 % (7 % considering quantum corrections) to the interfacial thermal transport at low temperatures (i.e., < 300 K), which is resulting from the stronger interference compared to scatterings among these phonons in the near-interface region. At high temperatures (i.e., > 300 K), phonon-phonon scattering plays a more important role than the phonon-phonon interference in the near-interface region, and therefore, the phonon-phonon couplings in the near-interface region hinder the interfacial thermal transport.

### CRediT authorship contribution statement

**Yixin Xu:** Writing – original draft, Visualization, Methodology, Investigation, Formal analysis, Data curation. **Bing-Yang Cao:** Writing – review & editing, Validation, Resources, Investigation. **Yanguang Zhou:** Writing – review & editing, Validation, Supervision, Resources, Investigation, Funding acquisition, Conceptualization.

### Declaration of competing interest

The authors declare that they have no known competing financial

### Appendix A. The calculation details of the heat current

As we discussed in Section 2.1, the heat current considering the phonon-phonon couplings across the interface and in the near-interface region is based on whether the atomic pair potential interaction  $U_{ij}$  involves atoms from both contact leads (i.e., thermal energy exchange across the interface) or only one lead (i.e., thermal energy exchange in the near-interface region).

For the systems in which all atoms are described using two-body potentials, as discussed in Section 2.1, the heat current resulting from the phonon-phonon couplings in the near-interface region is zero, and the near-interface effect on interfacial thermal transport can be ignored. For the Cu/Si with a mechanical-contacted interface (i.e., the interfacial interactions are described by two-body potentials while the Cu and Si atoms are depicted by many-body potentials), the partial function of the atomic potential involving atoms from both contacted sides can be directly written in the form of atomic force, i.e.,  $\frac{\partial U_i}{\partial \mathbf{r}_j} = \frac{1}{2} \frac{\partial U_{ij}}{\partial \mathbf{r}_{ij}} = \frac{1}{2} \vec{F}_{ij}$ . Therefore, the heat current considering phonon-phonon couplings across the mechanical-contacted Cu/Si interface depicted by the Lennard-Jones potential can be explicitly calculated using Eq. (14). However, the heat current considering the phonon-phonon couplings in the near-interface region needs to be calculated using Eq. (15) since the Si-Si and Cu-Cu interactions are both depicted by many-body potentials in which the partial potential functions (i.e.,  $\frac{\partial U_{ij}}{\partial \mathbf{r}_{ij}}$  and  $\frac{\partial U_{ij}}{\partial \mathbf{r}_{ij}}$ ) are affected by all their neighbors [17,38].

Here, we calculate the partial potential functions involving the many-body interactions using FDM [Eqs. (16) and (17)] ( $\Delta r_{ij}^x = \Delta r_{ij}^y = \Delta r_{ij}^z = 0.01\text{\AA}$ ), which inherently considers all many-body interactions. It is shown that the heat flux spectrum considering phonon-phonon couplings across the mechanical-contacted Cu/Si interface at 2 K calculated using FDM is identical to that calculated using the explicit interatomic force  $\frac{\partial U_i}{\partial \mathbf{r}_j} = \frac{1}{2} \frac{\partial U_{ij}}{\partial \mathbf{r}_{ij}} = \frac{1}{2} \vec{F}_{ij}$  (Fig. A1a). We also note that the heat flux spectrum considering phonon-phonon couplings in the near-interface region is not zero since  $\partial U_{ij} / \partial \mathbf{r}_{ij} \neq -\partial U_{ij} / \partial \mathbf{r}_{ji}$  (Fig. 3b). However, the heat flux considering phonon-phonon couplings in the near-interface region is quite small and can be ignored compared to that considering phonon-phonon couplings across the interface.

For the systems in which all atoms are depicted by many-body interactions, the heat current resulting from the phonon-phonon couplings in the near-interface region contributes non-negligible to the interfacial thermal transport (Fig. A1b), which is stemming from the largely asymmetric atomic environments in the near-interface region as we discussed above. Our calculated results clearly show that  $\vec{F}_{i \rightarrow i}$  is unequal to  $\vec{F}_{i \rightarrow i}$  (Fig. A2). As a result, the interfacial heat current for the systems described using many-body potentials should consider the phonon-phonon couplings across the interfaces and in the near-interface region. Furthermore, the integral of the total heat flux spectrum calculated based on FDM is equal to the heat flux in NEMD simulations, i.e.,  $J_{NEMD} = \frac{1}{A} \left\langle \frac{\partial E}{\partial t} \right\rangle$  (Fig. A1c).

It is noted that the spectral heat flux as shown in Fig. 6 is frequency dependent [32]. Therefore, the heat flux at a specific frequency stems from several vibrational modes with this specific frequency while various wavevectors. The peaks in Fig. 6 are related to the population, group velocities, and scatterings of vibrational modes with the same frequency. The trend of these peaks in Fig. 6 may be because of the number of transmitted vibrational modes at these frequencies. At the same time, we note that the peak value in the heat current spectrum does not necessarily follow a monotonical trend with the temperature (Figs. 5 and 6). This is because the peak value of the heat flux spectrum (Figs. 5 and 6) depends on the system heat current and the interfacial temperature drop, i.e.,  $Q(\omega, T) = G(\omega, T)\Delta T$ . On one hand, the system heat current  $Q$  is obtained by applying the temperature difference between the thermostats ( $T_{thermostats} = T \pm 0.4T$ ) in NEMD simulations. On the other hand, the temperature drops  $\Delta T$  at interfaces are also temperature-dependent since the interfacial thermal conductance  $G$  at various temperatures is different. Instead, we show that the interfacial thermal conductance and the corresponding quantum-corrected values follow the monotonical trend with temperature, as shown in Fig. 8.

interests or personal relationships that could have appeared to influence the work reported in this paper.

### Data availability

Data will be made available on request.

### Acknowledgement

Y.Z. acknowledges the startup fund (Grant No. REC20EGR14, a/c-R9246) and Frontier Technology Research for Joint Institutes with Industry Scheme (Grant No. FTRIS-002) from Hong Kong University of Science and Technology (HKUST). Y.Z. acknowledges the fund from Research Grants Council of the Hong Kong Special Administrative Region under Grant C7002-22Y, C6020-22 G, 26206023 and 16207124. Y. Z. thanks the fund from the Natural Science Foundation of Guangdong under Grant No. 306206039025. Y.Z. also thanks the Hong Kong Sci-Tech Pioneers Award from the Y-LOT foundation.

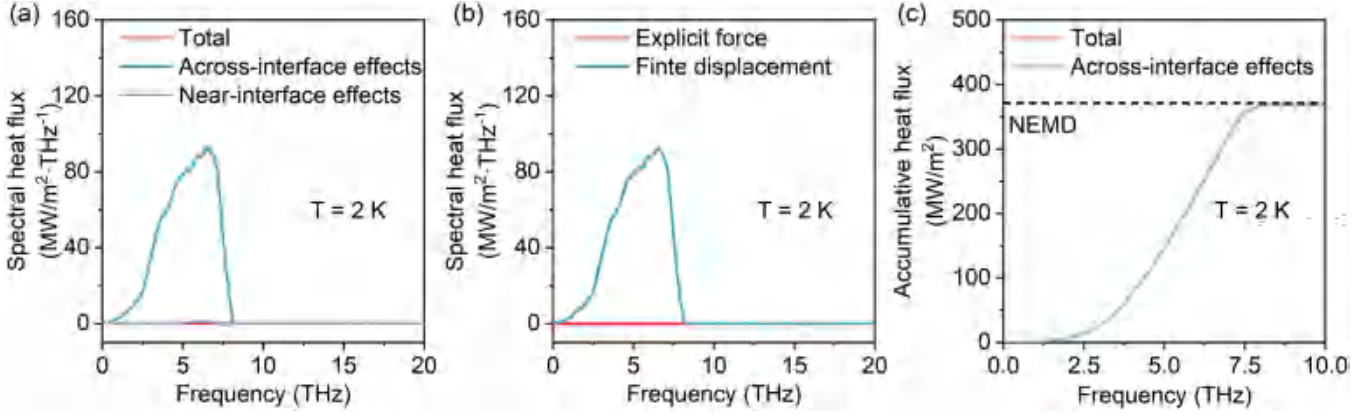


**Fig. A1.** (a) The spectral heat flux of mechanical-contacted Cu/Si interfaces at  $T = 2$  K. (b) The spectral heat flux resulting from the phonon-phonon couplings across the interface calculated using the explicit forces [Eq. (14)] and finite displacement method with  $\Delta r_{ij}^x = \Delta r_{ij}^y = \Delta r_{ij}^z = 0.01\text{\AA}$ , respectively. (c) The accumulative heat flux of (a) which is identical to the results calculated using the NEMD method, i.e.,  $J_{NEMD} = \frac{1}{A} \left\langle \frac{\partial E}{\partial t} \right\rangle$ . The red lines in (a) and (b) are guidance for eyes. (For interpretation of the references to colour in this figure legend, the reader is referred to the web version of this article.)

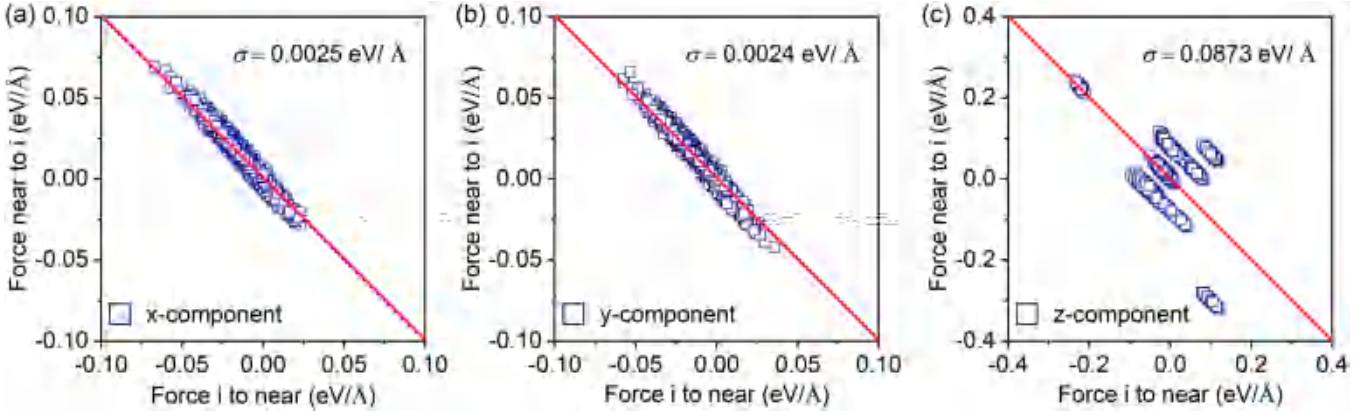


**Fig. A2.** Near-interfacial forces of the left or right interfacial region, the x-axis denotes the force exerted on the left (or right) interfacial atoms  $i$  by the left (or right) region, i.e.,  $\vec{F}_{i \rightarrow \bar{i}}$  in Eq. (15), and the y-axis denotes the force exerted on the left (or right) region by the left (or right) interfacial atoms  $i$ , i.e.,  $\vec{F}_{\bar{i} \rightarrow i}$  in Eq. (16). The standard deviation  $\sigma$  is given by  $\sigma = \sqrt{\frac{1}{N} \sum (f - \frac{1}{N} \sum f)^2}$ , in which  $f = F_{i \rightarrow \bar{i}}^\alpha + F_{\bar{i} \rightarrow i}^\alpha$  and  $\alpha$  is denoted as the x, y, and z component.

## Appendix B. The effects of the interfacial region

Here, we demonstrate that the interfacial region to calculate the thermal transport properties across the Cu/Si interfaces is large enough. Since the chemical-bonding Cu/Si interfaces have more obvious near-interface effects on the interfacial thermal transport, we consider the same interfacial region size for both mechanical-contacted and chemical-bonding Cu/Si interfaces in our simulations. The interfacial region applied to compute the spectral thermal transport properties should fully consider the near-interface effects, e.g., all the atoms contributing to the nonlinear temperature profile should be included, as discussed in Section 2.1. At the same time, Gordiz and Henry [12,34] have demonstrated that the vibrational properties in the near-interface region are different from that of its bulk counterpart. Our results here also show that the atomic vibrational density of state (VDOS) in the near-interface region is different from that of their bulk counterparts (Fig. B1). For instance, the high-frequency phonons ( $\sim 7.5$  THz for the Cu and  $\sim 15$  THz for the Si) at the contact atomic layers (labeled by 0.3 nm and 0.7 nm in Fig. B1) are largely reduced compared to that of their bulk counterparts (Figs. B1a and B1b). Furthermore, Feng *et al.* [37] indicate that these interfacial modes should be included when choosing the interface region for the spectral interfacial thermal transport analysis. Based on the discussions above, the length of the interfacial region for the Cu/Si interface should be at least 2.2 nm (Fig. B1), in which Cu and Si atoms are 0.9 nm and 1.3 nm away from the ideal interface, respectively.

We further calculate the spectral heat current considering phonon-phonon couplings across the interface [Eq. (19)] and in the near-interface region [Eq. (18)] using various interfacial regions. For the chemical-bonding Cu/Si interfaces, it is found that the heat flux spectrum becomes convergent when the thickness of the interfacial region is 2.2 nm (Fig. B2a), and the accumulation results are identical to the system heat current calculated using the NEMD method (Fig. B2b). Therefore, the interfacial region used to calculate the heat current spectrum in all our NEMD simulations is chosen to be 2.2 nm for Cu/Si interfaces.

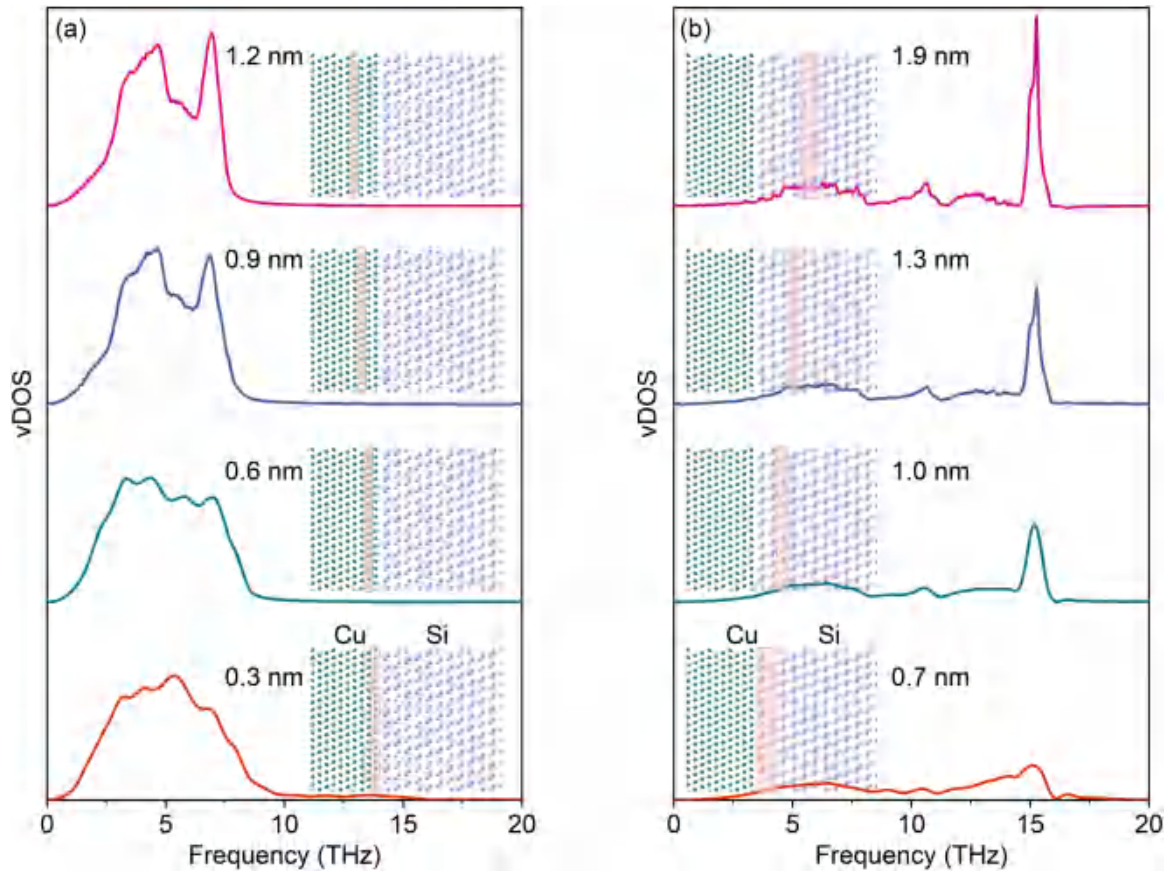


Fig. B1. Vibrational density of state of (a) Cu atoms and (b) Si atoms with their distance to the ideal interface varying from 0.3 nm to 1.2 nm and 0.7 nm to 1.9 nm, respectively.

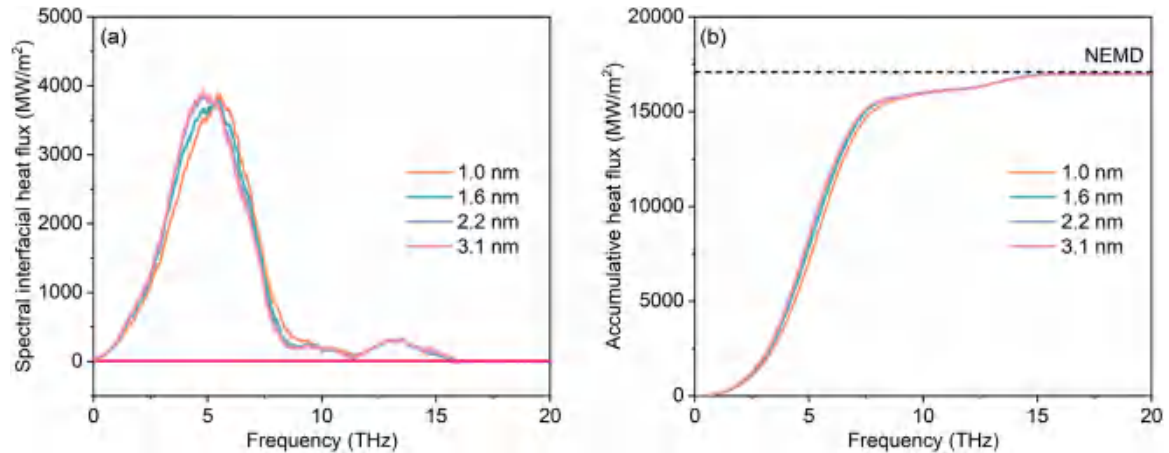


Fig. B2. (a) The heat flux spectrum and the accumulative heat flux considering phonon-phonon couplings and in the near-interface region of the chemical-bonding Cu/Si interfaces, calculated using different interfacial region sizes.

### Appendix C. Phonon transmission function in NEMD simulations

We have mentioned that all the phonon modes (i.e., normal modes) are intrinsically fully activated in classical MD simulations, even at extremely low temperatures [36,61,64]. Based on the Landauer theory, the heat current spectrum from the left lead to the right lead through a junction connecting two leads at two different equilibrium heat-bath temperatures (i.e.,  $T_L$  and  $T_R$ ) is written in the form of

$$Q(\omega, T) = \hbar\omega[n_L(\omega, T_L) - n_R(\omega, T_R)]\Gamma(\omega, T) \quad (C1)$$

where  $n$  is the equilibrium phonon distribution function at heat-bath temperatures and has the classical limit form of  $n_{L \text{ or } R}(\omega, T) = k_B T_{L \text{ or } R} / \hbar\omega$  in MD simulations, in which  $\Gamma(\omega, T)$  is the phonon transmission function or frequency-dependent transmission spectral density [7]. The spectral interfacial thermal conductance  $G(\omega, T)$  is then written as

$$\begin{aligned}
G(\omega, T) &= \lim_{T_L, T_R \rightarrow T} \frac{\hbar\omega[n_L(\omega, T_L) - n_R(\omega, T_R)]\Gamma(\omega, T)}{A(T_L - T_R)} \\
&= \lim_{T_L, T_R \rightarrow T} \frac{\hbar\omega\Gamma(\omega, T)}{A} \frac{\Delta n(\omega, T)}{\Delta T} \\
&\approx \frac{\hbar\omega\Gamma(\omega, T)}{A} \frac{\partial n(\omega, T)}{\partial T} \stackrel{\text{classical limit}}{=} \frac{k_B\Gamma(\omega, T)}{A}
\end{aligned} \tag{C2}$$

Therefore, the phonon transmission function in NEMD simulations can be calculated using  $\Gamma(\omega, T) = Q(\omega, T)/k_B\Delta T$  [16]. In our calculations, we first calculate the phonon transmission function using NEMD simulations, in which all the phonon modes are intrinsically assumed to be fully activated [64]. Then, we assume that the phonon modes follow the Bose-Einstein distribution, and the interfacial thermal conductance (i.e., referred to as quantum correction can be obtained via

$$G_{QC} = \frac{1}{2\pi A} \int_0^\infty \hbar\omega \frac{\partial f(\omega, T)}{\partial T} \Gamma(\omega, T) d\omega \tag{C3}$$

where  $f(\omega, T)$  is the phonon distribution function following the Bose-Einstein distribution, and  $\Gamma(\omega, T)$  is the phonon transmission function calculated by NEMD simulations. It is also worth noting that the scattering space for the phonon modes in MD simulations is also different from the realistic scattering space since phonons follow the classical limit of Boltzmann distribution in MD simulations [36,61,64]. Here, we only correct the distribution function for these phonons across the interface. We have demonstrated that the interfacial thermal transport properties calculated based on NEMD simulations after this quantum correction agree reasonably with the experimental measurements [16,65].

#### Appendix D. Temperature effect on the spatial cross-correlation function

We emphasize that the phonon interference only contributes to the interfacial heat current stemming from the phonon-phonon couplings in the near-interface region. The spatial cross-correlation functions at the near-interface regions of Cu/Si interfaces (Figs. 4 and 7) demonstrate that there exists interference among phonons caused by the intrinsic wave nature of these long-wavelength phonons rather than anharmonicity [59]. However, the spatial cross-correlation function is calculated based on the atomic vibrations, which therefore includes the effect of phonon-phonon scatterings. Therefore, at an extremely low temperature of 2 K, the phonon-phonon scatterings can be ignored, there is interference among these phonons with frequencies of 0~7.5 THz solely owing to the wave nature of phonons. Our spatial cross-correlation functions at the near-interface regions of mechanical-contacted Cu/Si interfaces (Fig. 4) demonstrate that there exists interference among phonons with frequencies ranging from 0~7.5 THz (i.e., the corresponding values are not zero). The vibrational transverse length at the near-interfacial region decreases when the temperature (i.e., phonon-phonon scatterings) is considered (Fig. D1). This agrees well with our calculated spectral ITC at temperatures (Fig. 3), in which the near-interface effects are dominated by the phonon-phonon scatterings.

Meanwhile, the spatial cross-correlation function captures the interference between phonons and only quantifies the specular transmitted waves ( $\omega_1 = \omega_2$  with the same direction, perpendicular to the interface) in our calculations [Eqs. (24)-(26)]. However, when calculating the heat current, we include the full-order phonon interactions as well as the inelastic and non-specular transmission (Fig. 7). Besides, the spectral heat current includes both the phonon-phonon scatterings and phonon-phonon interference resulting from the near-interfacial phonon-phonon interactions, which leads to the difference between the spatial cross-correlation function and the spectral heat flux.

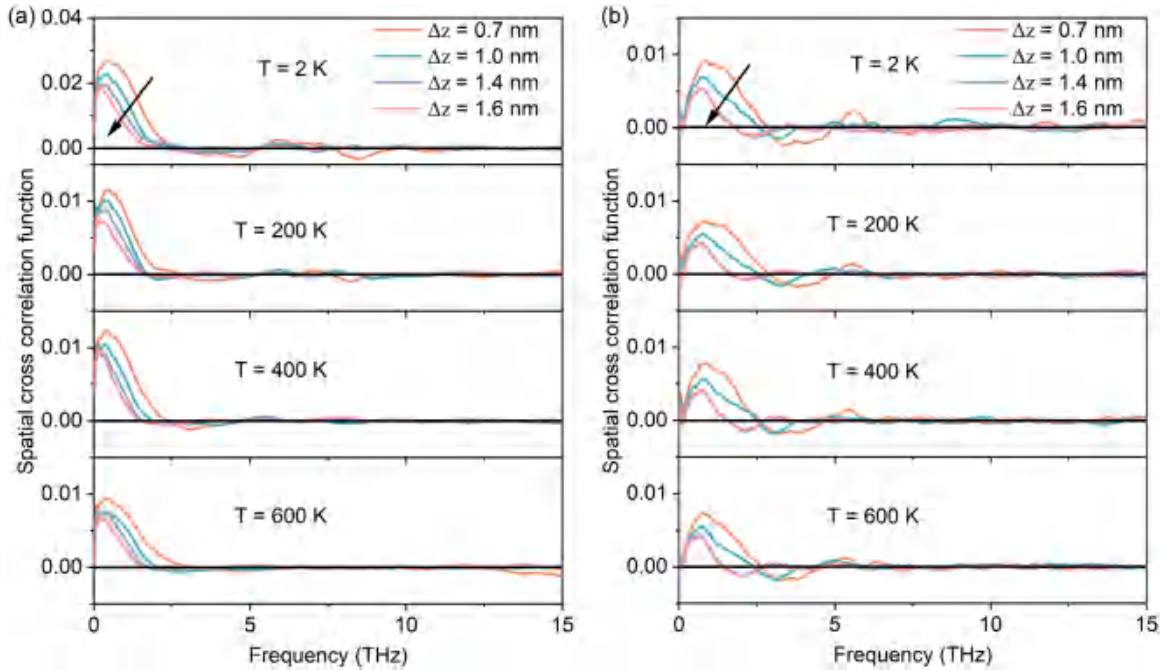


Fig. D1. Temperature effects on the spatial cross-correlation functions [Eq. (26)] at the near-interface regions of (a) mechanical-contacted Cu/Si interfaces and (b) chemical-bonding Cu/Si interfaces for vibrations transverse between Cu and Si leads.

## References

- [1] W.A. Little, The transport of heat between dissimilar solids at low temperatures, *Can. J. Phys.* 37 (1959) 334.
- [2] E.T. Swartz, R.O. Pohl, Thermal boundary resistance, *Rev. Mod. Phys.* 61 (1989) 605.
- [3] Y. Imry, R. Landauer, Conductance viewed as transmission, *Rev. Mod. Phys.* 71 (1999) S306.
- [4] C. Hua, X. Chen, N.K. Ravichandran, A.J. Minnich, Experimental metrology to obtain thermal phonon transmission coefficients at solid interfaces, *Phys. Rev. B* 95 (2017) 205423.
- [5] Y. Guo, Z. Zhang, M. Bescond, S. Xiong, M. Nomura, S. Volz, Anharmonic phonon-phonon scattering at the interface between two solids by nonequilibrium green's function formalism, *Phys. Rev. B* 103 (2021) 174306.
- [6] R.E. Peierls, *Quantum Theory of Solids*, Clarendon Press, 1955.
- [7] J. Chen, X. Xu, J. Zhou, B. Li, Interfacial thermal resistance: past, present, and future, *Rev. Mod. Phys.* 94 (2022) 025002.
- [8] T. Feng, W. Yao, Z. Wang, J. Shi, C. Li, B. Cao, X. Ruan, Spectral analysis of nonequilibrium molecular dynamics: spectral phonon temperature and local nonequilibrium in thin films and across interfaces, *Phys. Rev. B* 95 (2017) 195202.
- [9] Z. Cheng, et al., Experimental observation of localized interfacial phonon modes, *Nat. Commun.* 12 (2021) 1.
- [10] R. Qi, et al., Measuring phonon dispersion at an interface, *Nature* 599 (2021) 399.
- [11] H. Zhou, G. Zhang, Y.-W. Zhang, Effects of localized phonons on interfacial thermal conductance, *Phys. Rev. B* 106 (2022) 195435.
- [12] K. Gordiz, A. Henry, Phonon transport at crystalline Si/Ge interfaces: the role of interfacial modes of vibration, *Sci. Rep.* 6 (2016) 23139.
- [13] A. Rohskopf, R. Li, T. Luo, A. Henry, A computational framework for modeling and simulating vibrational mode dynamics, *Model. Simul. Mater. Sci. Eng.* 30 (2022) 045010.
- [14] Y. Zhou, M. Hu, Full quantification of frequency-dependent interfacial thermal conductance contributed by two- and three-phonon scattering processes from nonequilibrium molecular dynamics simulations, *Phys. Rev. B* 95 (2017) 115313.
- [15] A.K. Rappe, C.J. Casewit, K.S. Colwell, W.A. Goddard, W.M. Skiff, UFF, a full periodic table force field for molecular mechanics and molecular dynamics simulations, *J. Am. Chem. Soc.* 114 (1992) 10024.
- [16] Y. Xu, H. Fan, Z. Li, Y. Zhou, Signatures of anharmonic phonon transport in ultrahigh thermal conductance across atomically sharp metal/semiconductor interface, *Int. J. Heat Mass Transf.* 201 (2023) 123628.
- [17] J. Tersoff, Modeling solid-state chemistry: interatomic potentials for multicomponent systems, *Phys. Rev. B* 39 (1989) 5566.
- [18] J. Zhang, C. Liu, Y. Shu, J. Fan, Growth and Properties of Cu Thin Film Deposited on Si(001) Substrate: a Molecular Dynamics Simulation Study, *Appl. Surf. Sci.* 261 (2012) 690.
- [19] M. Kaviany, *Heat Transfer Physics*, 2nd ed., Cambridge University Press, Cambridge, 2014.
- [20] A.J.H. McGaughey, M. Kaviany, Phonon transport in molecular dynamics simulations: formulation and thermal conductivity prediction, in: *Advances in Heat Transfer*, 39, Elsevier, 2006, pp. 169–255, edited by G. A. Greene, J. P. Hartnett, A. Bar-Cohen, and Y. I. Cho.
- [21] J. Maassen, V. Askarpour, Phonon transport across a Si–Ge interface: the role of inelastic bulk scattering, *APL Mater.* 7 (2019) 013203.
- [22] Z. Zhang, Y. Guo, M. Bescond, J. Chen, M. Nomura, S. Volz, Heat conduction theory including phonon coherence, *Phys. Rev. Lett.* 128 (2022) 015901.
- [23] Z. Zhang, Y. Guo, M. Bescond, J. Chen, M. Nomura, S. Volz, Generalized decay law for particlelike and wavelike thermal phonons, *Phys. Rev. B* 103 (2021) 184307.
- [24] Z. Zhang, Y. Guo, M. Bescond, J. Chen, M. Nomura, S. Volz, How coherence is governing diffuson heat transfer in amorphous solids, *Npj Comput. Mater.* 8 (2022) 1.
- [25] M.N. Luckyanova, et al., Coherent phonon heat conduction in superlattices, *Science* (1979) 338 (2012) 936.
- [26] X. Qian, J. Zhou, G. Chen, Phonon-engineered extreme thermal conductivity materials, *Nat. Mater.* 20 (2021) 9.
- [27] B. Latour, S. Volz, Y. Chalopin, Microscopic description of thermal-phonon coherence: from coherent transport to diffuse interface scattering in superlattices, *Phys. Rev. B* 90 (2014) 014307.
- [28] R.J. Hardy, Energy-flux operator for a lattice, *Phys. Rev.* 132 (1963) 168.
- [29] Y. Xu, L. Yang, Y. Zhou, The interfacial thermal conductance spectrum in nonequilibrium molecular dynamics simulations considering anharmonicity, asymmetry and quantum effects, *Phys. Chem. Chem. Phys.* 24 (2022) 24503.
- [30] H.R. Seyf, K. Gordiz, F. DeAngelis, A. Henry, Using green-Kubo modal analysis (GKMA) and interface conductance modal analysis (ICMA) to study phonon transport with molecular dynamics, *J. Appl. Phys.* 125 (2019) 081101.
- [31] K. Gordiz, A. Henry, A formalism for calculating the modal contributions to thermal interface conductance, *New J. Phys.* 17 (2015) 103002.
- [32] Y. Zhou, M. Hu, Quantitatively analyzing phonon spectral contribution of thermal conductivity based on nonequilibrium molecular dynamics simulations. ii. from time Fourier transform, *Phys. Rev. B* 92 (2015) 195205.
- [33] K. Sääskilähti, J. Oksanen, J. Tulkki, S. Volz, Role of anharmonic phonon scattering in the spectrally decomposed thermal conductance at planar interfaces, *Phys. Rev. B* 90 (2014) 134312.
- [34] K. Gordiz, A. Henry, Phonon transport at interfaces: determining the correct modes of vibration, *J. Appl. Phys.* 119 (2016) 015101.
- [35] Y. Zhou, X. Zhang, M. Hu, Quantitatively analyzing phonon spectral contribution of thermal conductivity based on nonequilibrium molecular dynamics simulations. I. From space Fourier transform, *Phys. Rev. B* 92 (2015) 195204.
- [36] M. Puligheddu, Y. Xia, M. Chan, G. Galli, Computational prediction of lattice thermal conductivity: a comparison of molecular dynamics and Boltzmann transport approaches, *Phys. Rev. Mater.* 3 (2019) 085401.
- [37] T. Feng, Y. Zhong, J. Shi, X. Ruan, Unexpected high inelastic phonon transport across solid-solid interface: modal nonequilibrium molecular dynamics simulations and Landauer analysis, *Phys. Rev. B* 99 (2019) 045301.
- [38] Z. Fan, L.F.C. Pereira, H.-Q. Wang, J.-C. Zheng, D. Donadio, A. Harju, Force and heat current formulas for many-body potentials in molecular dynamics simulations with applications to thermal conductivity calculations, *Phys. Rev. B* 92 (2015) 094301.
- [39] Y.-X. Xu, H.-Z. Fan, Y.-G. Zhou, Quantifying spectral thermal transport properties in framework of molecular dynamics simulations: a comprehensive review, *Rare Met* 42 (2023) 3914.
- [40] P.L. Kapitza, Heat transfer and superfluidity of helium II, *Phys. Rev.* 60 (1941) 354.
- [41] J.B. Adams, S.M. Foiles, W.G. Wolfer, Self-diffusion and impurity diffusion of fee metals using the five-frequency model and the embedded atom method, *J. Mater. Res.* 4 (1989) 102.
- [42] S. Plimpton, Fast parallel algorithms for short-range molecular dynamics, *J. Comput. Phys.* 117 (1995) 1.
- [43] Y. Xu, G. Wang, Y. Zhou, Broadly manipulating the interfacial thermal energy transport across the Si/4H-SiC interfaces via nanopatterns, *Int. J. Heat Mass Transf.* 187 (2022) 122499.
- [44] M. Hu, X. Zhang, D. Poulikakos, C.P. Grigoropoulos, Large “near Junction” thermal resistance reduction in electronics by interface nanoengineering, *Int. J. Heat Mass Transf.* 54 (2011) 5183.
- [45] P. Erhart, K. Albe, Analytical potential for atomistic simulations of silicon, carbon, and silicon carbide, *Phys. Rev. B* 71 (2005) 035211.
- [46] Z. Cheng, et al., Thermal transport across ion-cut monocrystalline  $\beta$ -Ga<sub>2</sub>O<sub>3</sub> thin films and bonded  $\beta$ -Ga<sub>2</sub>O<sub>3</sub>-SiC interfaces, *ACS Appl. Mater. Interfaces* 12 (2020) 44943.
- [47] Z. Cheng, F. Mu, X. Ji, T. You, W. Xu, T. Suga, X. Ou, D.G. Cahill, S. Graham, Thermal visualization of buried interfaces enabled by ratio signal and steady-state heating of time-domain thermoreflectance, *ACS Appl. Mater. Interfaces* 13 (2021) 31843.
- [48] A.E.A. Bracesco, et al., The chemistry and energetics of the interface between metal halide perovskite and atomic layer deposited metal oxides, *J. Vac. Sci. Technol. A* 38 (2020) 063206.
- [49] N. Yang, T. Luo, K. Esfarjani, A. Henry, Z. Tian, J. Shiomi, Y. Chalopin, B. Li, G. Chen, Thermal interface conductance between aluminum and silicon by molecular dynamics simulations, *J. Comput. Theor. Nanosci.* 12 (2015) 168.
- [50] X. Li, J. Han, S. Lee, Thermal resistance from non-equilibrium phonons at Si–Ge interface, *Mater. Today Phys.* 34 (2023) 101063.
- [51] Z. Lu, Y. Wang, X. Ruan, Metal/dielectric thermal interfacial transport considering cross-interface electron-phonon coupling: theory, two-temperature molecular dynamics, and thermal circuit, *Phys. Rev. B* 93 (2016) 064302.
- [52] J.A. Thomas, J.E. Turney, R.M. Iutzi, C.H. Amon, A.J.H. McGaughey, Predicting phonon dispersion relations and lifetimes from the spectral energy density, *Phys. Rev. B* 81 (2010) 081411.
- [53] R. Peierls, Zur Kinetischen Theorie Der Wärmeleitung in Kristallen, *Ann. Phys.* 395 (1929) 1055.
- [54] A.J.H. McGaughey, M. Kaviany, Quantitative validation of the Boltzmann transport equation phonon thermal conductivity model under the single-mode relaxation time approximation, *Phys. Rev. B* 69 (2004) 094303.
- [55] J. Ravichandran, et al., Crossover from incoherent to coherent phonon scattering in epitaxial oxide superlattices, *Nat. Mater.* 13 (2014) 2.
- [56] P. Desmarchelier, E. Nikidis, R. Anufriev, A. Tanguy, Y. Nakamura, J. Kioseoglou, K. Termentzidis, Phonon diffraction and interference using nanometric features, *J. Appl. Phys.* 135 (2024) 015103.
- [57] M. Nomura, R. Anufriev, Z. Zhang, J. Maire, Y. Guo, R. Yanagisawa, S. Volz, Review of thermal transport in phononic crystals, *Mater. Today Phys.* 22 (2022) 100613.
- [58] S. Xiong, B. Latour, Y. Ni, S. Volz, Y. Chalopin, Efficient phonon blocking in sic antiphase superlattice nanowires, *Phys. Rev. B* 91 (2015) 224307.
- [59] M. Simoncelli, N. Marzari, F. Mauri, Unified theory of thermal transport in crystals and glasses, *Nat. Phys.* 15 (2019) 8.
- [60] C. Kittel, *Introduction to Solid State Physics*, 8th ed, Wiley, Hoboken, NJ, 2005.
- [61] Y. Zhou, Assessing the quantum effect in classical thermal conductivity of amorphous silicon, *J. Appl. Phys.* 129 (2021) 235104.
- [62] R. Landauer, Conductance from transmission: common sense points, *Phys. Scr.* 1992 (1992) 110.
- [63] S. Sadasivam, N. Ye, J.P. Feser, J. Charles, K. Miao, T. Kubis, T.S. Fisher, Thermal transport across metal silicide-silicon interfaces: first-principles calculations and green's function transport simulations, *Phys. Rev. B* 95 (2017) 085310.
- [64] J.E. Turney, A.J.H. McGaughey, C.H. Amon, Assessing the applicability of quantum corrections to classical thermal conductivity predictions, *Phys. Rev. B* 79 (2009) 224305.
- [65] Q. He, Y. Xu, H. Wang, Z. Li, Y. Zhou, Role of elastic phonon couplings in dictating the thermal transport across atomically sharp SiC/Si interfaces, *Int. J. Therm. Sci.* 204 (2024) 109182.